Limnol. Oceanogr., 41(8), 1996, 1629–1650

Pathways of carbon oxidation in continental margin sediments off central Chile

Bo Thamdrup and Donald E. Canfield[1]
Max Planck Institute for Marine Microbiology, Celsiusstr. 1, D-28359 Bremen, Germany

Abstract

Rates and oxidative pathways of organic carbon mineralization were determined in sediments at six stations on the shelf and slope off Concepción Bay at 36.5°S. The depth distribution of C oxidation rates was determined to 10 cm from accumulation of dissolved inorganic C in 1–5-d incubations. Pathways of C oxidation were inferred from the depth distributions of the potential oxidants (O_2, NO_3^-, and oxides of Mn and Fe) and from directly determined rates of SO_4^{2-} reduction. The study area is characterized by intense seasonal upwelling, and during sampling in late summer the bottom water over the shelf was rich in NO_3^- and depleted of O_2. Sediments at the four shelf stations were covered by mats of filamentous bacteria of the genera *Thioploca* and *Beggiatoa*. Carbon oxidation rates at these sites were extremely high near the sediment surface (>3 μmol cm^{-3} d^{-1}) and decreased exponentially with depth. The process was entirely coupled to SO_4^{2-} reduction. At the two slope stations where bottom-water O_2 was >100 μM, C oxidation rates were 10-fold lower and varied less with depth; C oxidation coupled to the reduction of O_2, NO_3^-, and Mn oxides combined to yield an estimated 15% of the total C oxidation between 0 and 10 cm. Carbon oxidation through Fe reduction contributed a further 12–29% of the depth-integrated rate, while the remainder of C oxidation was through SO_4^{2-} reduction. The depth distribution of Fe reduction agreed well with the distribution of poorly crystalline Fe oxides, and as this pool decreased with depth, the importance of SO_4^{2-} reduction increased. The results point to a general importance of Fe reduction in C oxidation in continental margin sediments. At the shelf stations, Fe reduction was mainly coupled to oxidation of reduced S. These sediments were generally H_2S-free despite high SO_4^{2-} reduction rates, and precipitation of Fe sulfides dominated H_2S scavenging during the incubations. A large NO_3^- pool was associated with the *Thioploca*, and the shelf sediments were thus enriched in NO_3^- relative to the bottom water, with maximum concentrations of 3 μmol cm^{-3}. The NO_3^- was consumed during our sediment incubations, but no effects on either C or S cycles could be discerned.

The mineralization of organic matter in the sea floor proceeds through a complex web of fermentative and respiratory microbial pathways where the oxidation of organic carbon to CO_2 is balanced overall by concomitant reduction of the inorganic electron acceptors O_2, NO_3^-, oxides of Mn and Fe, and SO_4^{2-}. To understand the regulation of carbon oxidation, independent quantification of each pathway would be ideal, but such quantification is only possible for a few of the pathways. The radiotracer technique for measuring SO_4^{2-} reduction rates (Jørgensen 1978) is one of the most robust methods available. Most importantly, SO_4^{2-} reduction is an entirely biological process that uses only organic substrates (and H_2) and has H_2S as the only immediate product. All of the other electron acceptors may be reduced in sediments either abiotically or through bacterial catalysis by one or more of the reduced inorganic species (H_2S, Fe^{2+}, Mn^{2+}, or NH_4^+), and no technique is available for measuring organotrophic respiration alone. Hence, the quantification of these processes relies on multilateral approaches wherein different types of measurements together constrain the rates.

Determinations of bacterial SO_4^{2-} reduction rates in sediments are numerous and have shown that this pathway accounts for 10–90% of the C oxidation in coastal sediments, with 50% as a median value (Jørgensen 1982; Henrichs and Reeburgh 1987; Canfield 1993). Most of the sulfide produced from SO_4^{2-} reduction is typically reoxidized within the surface sediment rather than being buried. Thus, although benthic O_2 uptake provides a good estimate of sediment metabolism in most continental margin sediments, a significant part of this O_2 consumption is typically not directly coupled to C oxidation, but instead is coupled to the reoxidation of inorganic compounds such as H_2S (Jørgensen 1982). No technique is presently available for direct quantification of aerobic respiration in sediments.

Several methods have been used for measuring sedimentary NO_3^- reduction (Sørensen 1978; Seitzinger et al. 1984; Nielsen 1992), with results that generally demonstrate a minor role (≤10%) for C oxidation in coastal sediments (Sørensen et al. 1979; Canfield et al. 1993*a*). The significance for C oxidation may be higher in areas with low O_2 and (or) elevated NO_3^- concentrations in the bottom water (cf. Canfield 1993).

The contributions of Mn and Fe reduction to C oxidation are the most infrequently quantified of the respi-

[1] Present address: Institute of Biology, University of Odense, DK-5230 Odense M, Denmark.

Acknowledgments

We are grateful to Henrik Fossing, Victor Ariel Gallardo, and Bo Barker Jørgensen for initiating, organizing, and leading the Thioploca Expedition 1994 and to Kirsten Neumann and Swantje Fleischer for skillful technical assistance. We also thank the Captain and crew of RV *Vidal Gormaz* as well as all members of the scientific party for good company and collaboration during the expedition and for permission to cite unpublished results from the cruise. The comments of the reviewers are appreciated.

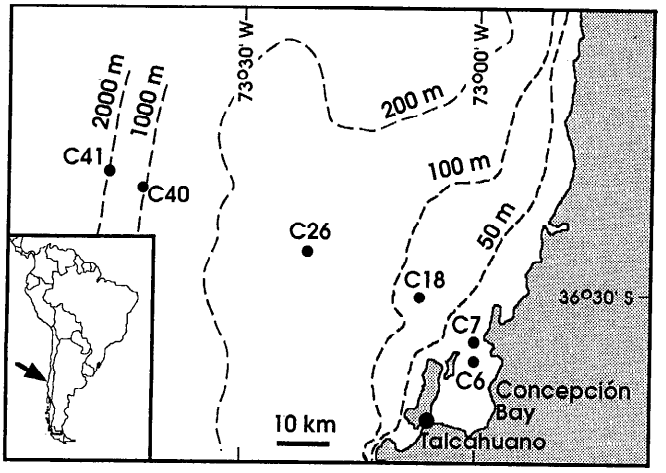

Fig. 1. Map showing sampling locations.

ratory types. Estimates based on pore-water gradients of Mn^{2+} and Fe^{2+} have found the processes to be of little importance (e.g. Bender and Heggie 1984; Reimers et al. 1992). In the presence of sediment and pore-water transport by bioturbation, however, such estimates underestimate actual turnover rates (Aller 1980; Canfield 1993), and a further complication arises from the adsorption or precipitation of reduced Mn and Fe (Canfield et al. 1993*b*; Thamdrup et al. 1994*a*). Indeed, Aller (1990) found that in Mn oxide-rich sediments of the Panama Basin, Mn reduction dominated C oxidation and that the process was supported by bioturbation, which mixed the oxides and organic matter into anoxic sediment layers.

A major difficulty in quantifying dissimilatory Mn and Fe reduction arises from the competing abiotic reactions with H_2S and, for Mn oxides, with Fe^{2+} (Pyzik and Sommer 1981; Postma 1985; Burdige and Nealson 1986). Reaction with H_2S may be so rapid that this compound may be undetectable even in sediments with high rates of SO_4^{2-} reduction (Goldhaber and Kaplan 1974; Canfield et al. 1992). Reaction with H_2S was found to dominate Fe reduction in a coastal bay, with dissimilatory Fe reduction contributing <5% to C oxidation (Thamdrup et al. 1994*a*). Similar conclusions have been reached for Mn reduction in a number of relatively Mn-poor sediments (Canfield et al. 1993*b*; Aller 1994; Thamdrup et al. 1994*a*).

By contrast, Sørensen (1982) showed that in oxidized sediment, Fe reduction proceeded through biological catalysis and was independent of SO_4^{2-} reduction. Furthermore, from the depth distribution of O_2, NO_3^-, and rates of SO_4^{2-} reduction in some coastal sediments, a zone dominated by Fe reduction has been suggested (Sørensen and Jørgensen 1987; Hines et al. 1991). In a study of three sites in the Norwegian Trough, Canfield et al. (1993*b*) compared total mineralization rates to SO_4^{2-} reduction rates in anoxic sediment incubations. Based on excess total mineralization relative to the mineralization due to SO_4^{2-} reduction, Fe reduction was found to contribute 44 and 69% of anaerobic C oxidation at two sites, whereas at the third site, essentially all mineralization was coupled to Mn reduction. These large contributions were associated with strong bioturbation and, in the last case, with a very high Mn oxide content. From comparison with benthic O_2 uptake rates, it was concluded that the anaerobic processes dominated C oxidation, whereas aerobic respiration contributed only 4–17%; furthermore, it was suggested that the role of aerobic respiration in C oxidation has generally been overestimated in continental margin sediments (Canfield et al. 1993*a*).

Table 1. Positions and bottom-water data for stations sampled 12–23 March 1995 (nd—not detected).

	Position (36°S+, 73°W+)	Depth (m)	Temp (°C)	O_2* (μM)	NO_3^- (μM)
C6	37.3'S, 00.5'W	34	11.4	nd	3
C7	36.5'S, 00.6'W	37	11.6	nd	21
C18	30.8'S, 07.7'W	87	11.7	nd	18
C26	25.9'S, 23.4'W	122	11.2	nd	15
C40	20.1'S, 43.7'W	1,015	6.0	105	43
C41	19.6'S, 49.3'W	2,000	3.9	220	35

* Data provided by J. K. Gundersen and R. N. Glud.

Although the studies cited above have provided the first evidence on the diversity of C oxidation pathways, it is also clear that a general understanding of the relative importance of these pathways and their regulation in sediments has not been reached. We have applied an approach similar to that of Canfield et al. (1993*b*) to sediments from the upwelling region off central Chile. Stations were chosen on a transect that ran from a highly productive shelf area with O_2-deficient bottom waters to halfway down the continental slope. This approach gave us an opportunity to study how the pathways of C oxidation responded to variations in bottom-water O_2 levels. This study extended the small database on the significance of dissimilatory Fe and Mn reduction and also served as a further test of the methodology.

Study area

As part of the "*Thioploca* Cruise 1994" onboard RV *Vidal Gormaz* (Fossing et al. 1995), sediments were collected on the continental margin off Concepción Bay (Fig. 1, Table 1). Stations were distributed along a transect from the mouth of the Bay at 34-m depth, across the 40-km-wide shelf, to 2,000-m depth on the slope. The region is characterized by a very high upwelling-driven primary production during summer (September–April), with upwelling induced by south–southwest winds that typically blow for periods of a week, followed by a few days of calm or north winds (Ahumada et al. 1983; Arcos and Wilson 1984; Peterson et al. 1988). The noncontinuous upwelling pattern causes strong temporal variations in primary productivity. Sediments were sampled during late summer (12–23 March), and upwelling-favorable winds blew throughout the first half of March.

A pronounced O_2 minimum zone is associated with the south-flowing equatorial subsurface water, which is found at 100–400-m depth in nonupwelling periods (Brandhorst 1959; *see* Sobarzo 1994). During summer upwelling, this

water mass may reach 20-m depth and may cover the shelf and reach into the Concepción Bay, thereby reducing bottom-water O_2 concentrations over the shelf (Ahumada et al. 1983; Peterson et al. 1988). Thus, O_2 concentrations <11 μM have been reported from the shelf bottom water during this season (Roa et al. 1995). Inside the bay, bottom-water anoxia, H_2S release, and faunal mass mortality are recurring phenomenona (Ahumada et al. 1983). During the sampling period, an O_2-deficient zone was found at 100–300-m depth offshore, and it stretched up over the shelf to 30–40-m depth, so that all shelf sediments studied were fully anoxic (Table 1; R. N. Glud et al. in prep.).

Sedimentation rates from ^{210}Pb distributions at stations C41, C40, C18 (Fig. 1), and at locations close to C6 and C7, all fall in the range 1–2.2 mm yr^{-1} (mean, 1.2; M. Salamanca pers. comm.). Giant filamentous bacteria of the genus *Thioploca* were first described from the shelf sediments outside the bay, where they occur in matlike masses in the O_2 minimum zone (Gallardo 1977). On the inner shelf, where O_2 levels vary strongly over the year, the mats proliferate in summer and may break up and become exported with bottom currents during winter (V. A. Gallardo pers. comm.). Single filaments are up to 40 μm wide and 7 cm long (Fossing et al. 1995) and are found in conspicuous (up to 1.5-mm-thick) sheathed bundles. These filaments belong to the species *Thioploca chilea* and *Thioploca araucae* (Maier and Gallardo 1984*a*; Teske et al. 1996). Sulfide oxidation has been proposed as their main method of metabolism (Maier and Gallardo 1984*b*), but despite wide distribution of these species in the Chilean and Peruvian upwelling areas (Gallardo 1977), their ecology is poorly known and was a main subject of investigation during the cruise (Fossing et al. 1995).

Methods

The sediments were sampled with a multiple corer (Barnett et al. 1984) that retrieved up to eight cores in polycarbonate liners of 9.6-cm i.d, although for stations C7 and C40, a 30 × 30-cm box core was subsampled into such liners on deck. Cores were only accepted when the surface appeared neither affected by resuspension nor, in presence of surface mats, disrupted or pushed down during coring. Cores were immediately transferred to an incubator set at bottom-water temperature (Table 1).

Sediment incubation and pore-water extraction—For the pore-water chemistry, one or two cores were processed, generally within 1 h of retrieval. In an N_2-filled glove bag, the sediment was sectioned in appropriate intervals and loaded into polypropylene centrifuge tubes. The tubes were tightly capped and centrifuged for 5–10 min, and after reintroduction into the glove bag, the pore water was sampled and filtered through Whatman GF/F glass-fiber filters. Conservation and analyses of samples are described below.

A finer spatial resolution of the NO_3^- distribution near the sediment surface was attempted with a whole-core squeezer (Bender et al. 1987). Pore water was extruded by driving the sediment core from below toward a stationary lid with a central 1-mm-wide hole covered with a paper filter. Water was collected in 2-ml aliquots, each corresponding to ~0.9-mm depth in the core, depending on porosities.

For the determination of carbon mineralization rates and pathways, sediment from the upper 10 cm of six cores (434 cm^2 in total) was incubated as described by Canfield et al. (1993*b*) in laminated ethyl-vinyl-alcohol plastic Würgler bags (Ril-O-Ten; Hansen 1992; Kruse 1993) after it had been sectioned into eight depth intervals and the parallel intervals from different cores were mixed. Sediments were processed over ~2 h in an N_2-filled glove bag beginning within 4 h of retrieval. The incubation bags were first closed with a big clip, which eliminated any head space, and they were then heat-sealed behind the clip, thus avoiding heating of the sediment. The bags were incubated dry at bottom-water temperature (Table 1) and, in addition to the initial sample, sampled four times at regular intervals in the glove bag. Apart from the initial exposure during loading, the bags were exposed to room temperature (~18°C) for <10 min during samplings to avoid temperature artifacts on rates. The generally linear accumulation of metabolites during our incubations argues against any significant transient stimulation of metabolic activity resulting from initial sample heating and handling. During incubation, the bags were not placed in a larger N_2-filled bag as practiced by Canfield et al. (1993*b*). The range of oxygen permeability reported for the plastic (Hansen 1992; Kruse 1993) at a maximum bag surface : volume ratio of 0.2 m^2 $liter^{-1}$ corresponds to an oxygen input of 1–4 nmol cm^{-3} d^{-1}, which is insignificant for the metabolically active sediments studied here. Generally, however, we recommend the use of an outer anoxic bag for sediment incubations.

For stations C7–C26, the total incubation time was 30–35 h; station C40 was incubated for 4 d and C41 for 5 d. At station C6, the incubation was ended after the second sampling (5-h incubation) because of incubator failure. With stations C7 and C18, we prolonged the incubations to 6 and 10 d, respectively, to monitor long-term changes in the pore water and solid phases. For each sampling, sediment was loaded into centrifuge tubes and pore water was retrieved under N_2 as described above.

During the short-term incubations, rates of sulfate reduction were determined once at C6 and C7 and twice at all other sites in splits of 10-ml sediment with $^{35}SO_4^{2-}$ tracer (Jørgensen 1978) in 3-h (shelf sites) to 10-h (C41) incubations at the same temperature as the bags. For termination, the sediment was fixed in 20% zinc acetate and frozen. The reduced ^{35}S was recovered by distillation with boiling acidic Cr^{2+} solution (Zhabina and Volkov 1978; Canfield et al. 1986; Fossing and Jørgensen 1989).

At the end of the short-term incubations, pore-water pH was determined with a glass electrode that was inserted into subsamples of the sediment and was calibrated with NBS standards.

Pore-water analyses—Portions of pore water for ΣCO_2 (dissolved inorganic carbon) and NH_4^+ analyses were filtered into 1.8-ml glass vials that were capped with Teflon-

coated butyl rubber septa, leaving no gas phase and maintaining anoxia. The samples were stored at 4°C and analyzed right after termination of the short-term incubations or, for the pore-water cores, within 5 d by means of flow-injection systems with gas-exchange and conductivity detection for both species (Hall and Aller 1992; SD 2% for both). Although we cannot exclude slight ΣCO_2 production from DOC oxidation during the brief storage, we expect this to be insignificant relative to the production in the sediments given the storage conditions. Samples that contained H_2S from C6 and samples from prolonged incubations at C7 and C18 that contained H_2S were first analyzed for NH_4^+ and then treated with 5% vol of a 10% H_2O_2 solution (R. C. Aller pers. comm.). This treatment removed all H_2S within 10 min and had no effect on ΣCO_2 measurements, as determined from similarly treated standards.

Pore water for determination of $NO_3^- + NO_2^-$ was stored frozen. For analysis, NO_3^- was reduced to NO_2^- by shaking the sample with spongy cadmium, and total NO_2^- was subsequently determined (Jones 1984). Tests showed that 3 h of reaction ensured complete reduction to NO_2^- without overreduction to NH_4^+.

Dissolved Fe^{2+} in the pore-water cores was determined immediately after filtration by colorimetry with a Ferrozine solution without reducing agent (det. limit 1 μM; SD 2%; Stookey 1970), whereas pore-water Fe^{2+} in the incubated sediment was determined in acidified samples at the end of the incubation. Dissolved Mn^{2+} and Ca^{2+} were analyzed in acidified pore water by flame atomic absorption spectroscopy (Mn^{2+} det. limit 0.5 μM; SD 2% for both).

Sulfate was determined by nonsuppressed anion chromatography (SD 1%). Samples for H_2S analysis (100–300 μl) were fixed immediately in 50 μl 20% Zn acetate and frozen for later analysis by the methylene blue method (det. limit 1 μM; SD 5%; Cline 1969).

Solid-phase analysis—Portions of sediment from the beginning of the incubations and the sediment remaining in the bags at the end were sampled under N_2, frozen, and later analyzed for solid Fe, Mn, and S phases. Iron was extracted with dithionite-citrate-acetic acid (DCA; pH 4.8; Lord 1980; Canfield 1989) and acidic ammonium oxalate (pH 3.0; Schwertmann 1964). DCA extracts all free iron oxides (except some magnetite; Canfield 1988; 1989) together with Fe(II) phases such as FeS and $FeCO_3$ (Thamdrup et al. 1994*a*; Kostka and Luther 1994) but does not allow a separate determination of Fe(III) and Fe(II). Oxalate has been used to extract poorly crystalline Fe oxides from soils and sediments (Schwertmann 1964; Canfield 1988, 1989). Its selectivity is, however, dependent on the absence of Fe^{2+}, because the Fe^{2+}-oxalate complex efficiently catalyzes the dissolution of crystalline Fe(III) phases (Fischer 1973; Suter et al. 1988). Because ferrous phases such as FeS and $FeCO_3$ are also dissolved by this extraction, unwanted dissolution of unreactive Fe(III) phases from anoxic Fe(II)-bearing sediments results (Thamdrup et al. 1994*a*; Kostka and Luther 1994). To avoid this catalytic interference of Fe^{2+}, we air-dried the sediment before extraction, thereby oxidizing FeS and $FeCO_3$ to ferrihydrite (Canfield 1988, 1989; Raiswell et al. 1994). Calibration experiments with pure Fe phases mixed into dried sediment confirmed the selectivity towards poorly crystalline oxides (D. E. Canfield unpubl.). In parallel with the (oxic) extraction of dried sediment, Fe^{2+} was determined in an anoxic oxalate extraction of fresh (frozen) sediment (Phillips and Lovley 1987) in order to quantify the contribution of Fe(II) phases to the oxalate-extractable Fe. Oxalate-extractable Fe(III) was defined as the difference between these two measures.

We used 10-ml extractants with ~150 mg wet or 50 mg of dry sediment. Extraction times were 1 h for DCA and 4 h for oxalate, and the extraction conditions were otherwise as described by Canfield et al. (1993*b*) and Thamdrup et al. (1994*a*). Total extractable Fe and Fe(II) were determined with Ferrozine (above references). Manganese was determined in the DCA extracts by flame AAS.

Acid-volatile sulfide (AVS = FeS + H_2S) and chromium-reducible sulfur (CRS = FeS_2 + S^0) were determined after a two-step distillation with cold 2 N HCl and boiling 0.5 M Cr^{2+} solution (Fossing and Jørgensen 1989). Elemental sulfur was extracted by shaking the samples with methanol for 24 h and was then determined with HPLC (T. G. Ferdelman et al. unpubl.). For this determination, sediment fixed with Zn acetate from the SO_4^{2-} reduction measurements was used. Concentrations of FeS and FeS_2 were calculated as AVS − H_2S and (CRS − S^0)/2, respectively.

Organic C and total N and S were determined in dried sediment on an elemental analyzer (Carlo Erba; SD 2%); inorganic C was removed by acidification (HCl) and drying of the sample boats prior to analysis. Inorganic C in carbonates was determined by acidification of 0.1–0.5 g of dried sediment with 10 ml of 4 M HCl in 120-ml serum bottles and measurement of the evolved CO_2 in the headspace by gas chromatography with thermal conductivity detection (SD 5%). These values were corrected for carbonate alkalinity.

Thioploca *analysis and* NO_3^- *extractions*—For determination of the bulk composition of *Thioploca*, a 10-cm-deep sediment core with a well-developed mat at the surface was sieved (1 mm) and washed with surface seawater. Remaining detritus and macrofauna were removed with forceps, leaving a visually clean pellet of sheathed *Thioploca*, which was then frozen. About 1 g wet wt of *Thioploca* was freeze-dried and ground for analysis. Organic C, N, and S were determined with an elemental analyzer as above. The NO_3^- content was analyzed as described below. To estimate the contribution of salt to the dry weight, Cl^- was extracted in water and analyzed by ion chromatography. The total salt content was calculated from Cl^- and the typical composition of seawater.

Because we discovered during the cruise that *Thioploca* concentrated NO_3^- far beyond pore-water concentrations, an NO_3^- extraction of total sediment was tested and applied. Drying and rewetting had proven to be an efficient way to release NO_3^- from single filaments of

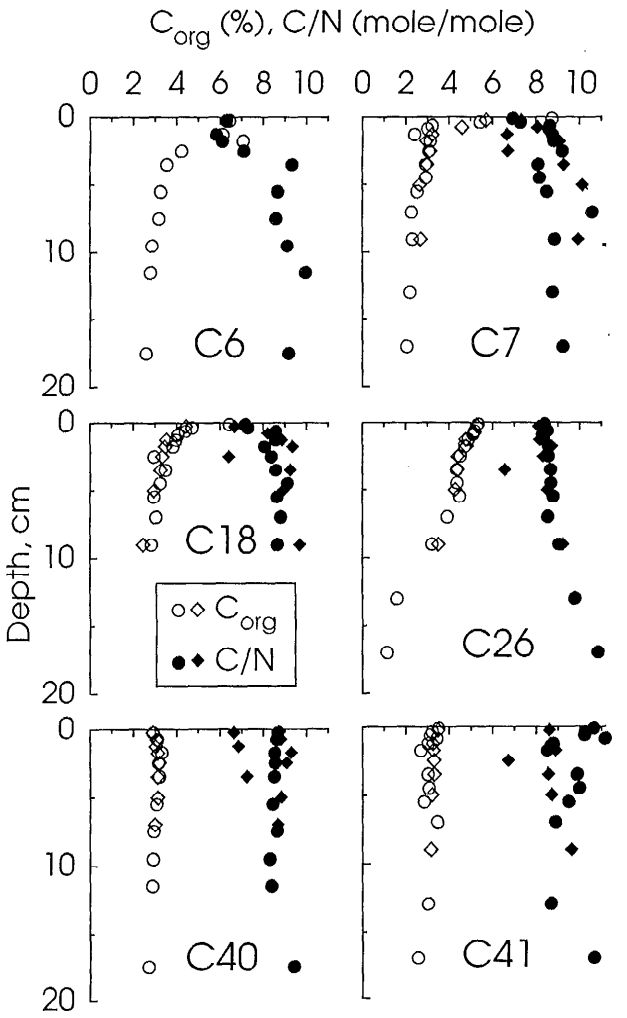

Fig. 2. Depth distributions of organic carbon and C_{org} : N ratios. Data both from sediment used for incubations (diamonds) and from a core for pore-water analysis (circles) are shown.

Thioploca (L. P. Nielsen pers. comm.). For the extraction, frozen sediment was dried either at 80°C after brief thawing or in a freeze-drier that avoided thawing completely. The sediment was ground by hand and 50–100 mg (5 mg for *Thioploca* samples) was then extracted in 10 ml water for 15 min. After centrifugation, NO_3^- in the supernatant was determined as in the pore-water samples. The extraction procedure was tested with surface sediment from the NO_3^- rich C7. Large and highly reproducible amounts of NO_3^- were released in the first 15-min extraction, and the yield decreased sharply in a second wash. The release of NO_3^- decreased little in three further washes and stabilized at concentrations ~0.2 μmol g^{-1}, corresponding to 1–2 μM in the extract independent of the yield in the first wash. Extraction in 1 M KCl or sonication during the extraction did not increase the yield (data not shown). Also, extraction of the deepest sediment sections and of sediment from the prolonged incubations, where strongly reducing conditions developed, consistently yielded non-zero NO_3^- concentrations around the "background" level of the test extractions (*see below*). We interpret this stable background concentration as an artifact for which we have no certain explanation, but which could be the result of nitrification during the extraction. This background was subtracted in calculations of NO_3^- pool sizes.

Results

Sediment description—White filamentous bacteria (*Thioploca* spp. and *Beggiatoa* spp.) were observed in masses in the anoxic shelf sediments and in mats formed on the surface. The sediment at station C6 was black and sulfidic and had a web of *Beggiatoa* filaments practically floating on 2 cm of fluff that graded into silt. At C7 and C18, ~2-cm-thick matlike structures containing *Thioploca*, the small suspension feeding polychaete *Paraprionospio pinnata* (~1 cm), and juvenile squat lobsters, *Pleuroncodes monodon* (~1 cm) were observed on the surface of the otherwise silty, dark brown sediments. Single strands of *Thioploca* and a few burrows of larger polychaetes were seen to 10-cm depth. Station C26 did not have a distinct bacterial mat at the surface, but strands of *Thioploca* were distributed within the upper 10 cm. This sediment consisted of green silt to 10–15-cm depth and gray clay with a purple tinge below this level. At the slope stations, the sediment was brown and silty and infauna was indicated by burrow structures.

Solid phase and pore-water chemistry—To facilitate direct comparison of rates and pool sizes, concentrations of solids (except C_{org} and N) are given on a volume rather than on a dry weight basis. To some extent, this choice masks changes that occur within the solids, because a component that makes up a constant fraction of the solids increases with depth solely owing to compaction. This masking effect is particularly significant at the inner sites, where porosities decreased from >0.95 in the surface mat to ~0.85 at 10-cm depth.

The distribution of the organic C and the C_{org} : N ratio in the sediments are shown in Fig. 2. Only the surface layers showed pronounced changes through the transect, with high C_{org} concentrations of up to 8% dry wt at the shallower stations decreasing to ~3% at the slope stations. A concentration ~3% was also approached in the deeper parts of the shelf cores. At C26, C_{org} was ~4% in the upper 10 cm and dropped to 1% below this. This change coincided with the abrupt color change from green to gray. The station also stood out with respect to other solid components (*see below*). Low C_{org} : N ratios of 6–7 were associated with the high C_{org} in the mats; otherwise, values were ~9.

The distribution of inorganic carbon (ΣCO_2) and NH_4^+ in the pore waters showed a uniform trend along the transect, and the extremely steep concentration gradients and strong convex curvature of the profiles at the nearshore stations indicated high rates of C mineralization (Fig. 3). Offshore, both the surface gradients and the curvature of the concentration profiles decreased dramatically. The ΣCO_2 and NH_4^+ distributions were generally parallel. At C7 and in one core at C18, however, a preferential release of NH_4^+ was indicated near the surface.

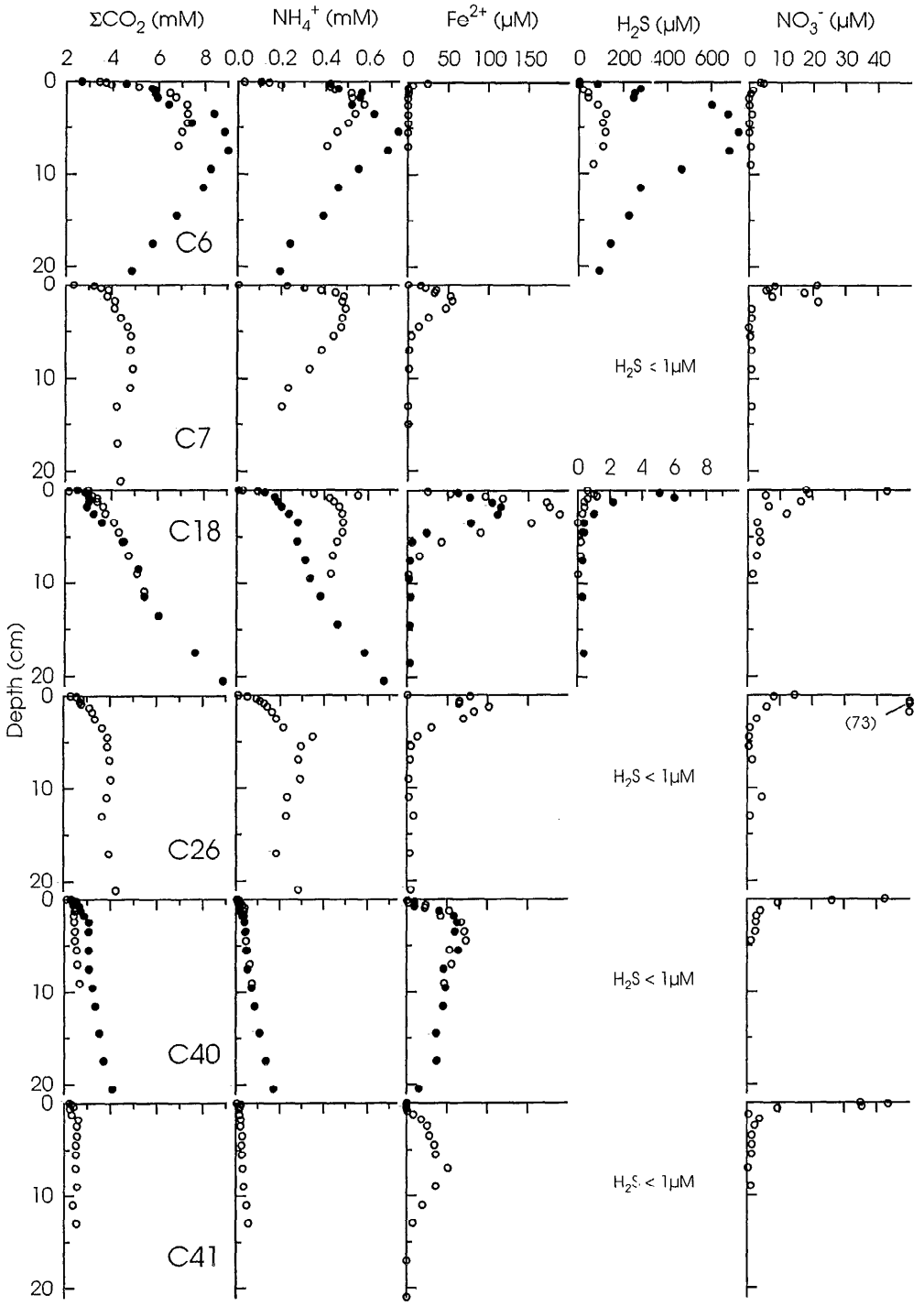

Fig. 3. Depth distributions of dissolved species from the shallowest (C6, top) to the deepest (C41, bottom) site. At stations C6, C18, and C40, two cores were analyzed, which are distinguished by the use of open and filled circles.

Potential oxidants for C_{org}: O_2 and NO_3^-—Bottom-water oxygen was available only on the slope, where it penetrated into the sediment to 6 mm at C40 and to 8 mm at C41 (Table 1; J. K. Gundersen and R. N. Glud pers. comm.). The penetration for C40 was obtained in situ with oxygen electrodes mounted on a benthic lander (Gundersen and Jørgensen 1991) and that for C41 was measured in a core incubated at bottom-water temperature and O_2 concentration onboard ship (Glud et al. 1994).

Nitrate was ≥ 15 μM in the bottom water at all stations

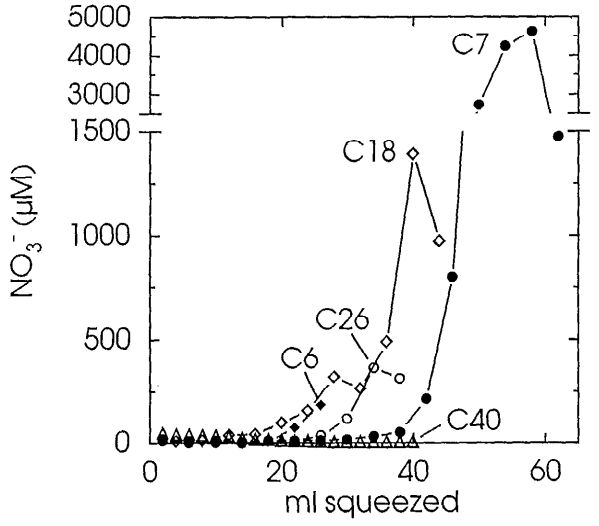

Fig. 4. Nitrate concentration in fractions collected from whole-core squeezing of sediment from five stations. Two milliliters corresponds to ~0.9-mm depth in the core.

except C6 (Table 1). As defined from centrifuged sediment, pore-water NO_3^- penetrated to 5 mm at C6, 1.5–2 cm at the other shelf stations, and to 1 cm on the slope (Fig. 3). For the shelf stations (C7–C26), NO_3^- profiles were characterized by an irregular shape and by several values well above the bottom-water concentration. Attempts to obtain profiles at a finer spatial resolution by means of a whole-core squeezer, which has been used successfully for NO_3^- with other sediments (Bender et al. 1987; Brandes and Devol 1995), produced even stranger results. We observed that the concentration of NO_3^- in the collected pore water increased with virtual depth as the squeezing proceeded and more pressure was applied, reaching up to 5 mM (Fig. 4). Such effects were not observed with the slope sediments. Analysis of single filaments of *Thioploca* showed that these bacteria may concentrate NO_3^- in their large central vacuole (Fossing et al. 1995); therefore, centrifuging pore water or squeezing sediment may lead to elevated pore-water NO_3^- concentrations by disrupting cells.

In Table 2, the total amount of NO_3^- released from the sediments by whole-core squeezing is compared to that measured in the pore water after centrifugation. For C6–C18 the whole-core-squeezed sediment contained far more NO_3^- than did the centrifuged pore water, but we were not certain that most NO_3^- in the sediment was even released by the whole-core squeezing. As an alternative estimate of the sediment NO_3^- pool, we therefore extracted NO_3^- from dried sediment. The depth distribution of extractable NO_3^- (Fig. 5) confirmed that at the *Thioploca* mat stations C18 and in particular C7, much more NO_3^- was present in the sediment than was measured in the pore water (Table 2). Although the pool of extractable NO_3^- was 5 times larger than the pore-water pool at these stations, it still represented only half the pool extruded by whole-core squeezing. It was surprising that whole-core squeezing provided the highest estimates

Table 2. NO_3^- pool size measured with different methods (mmol m^{-2}) (nd—not detected; nm—not measured).

	Pore-water centrifugation	Whole-core squeezing	Drying and extraction
C6	0.1	1.6	0.3
C7	0.3	26.9	16.9
C18	0.6	7.2	3.3
C26	0.8	0.6	1.7
C40	0.2	0.3	nm
C41	0.3	0.2	nd

of the sedimentary NO_3^- content at the *Thioploca* mat stations, because the pattern of NO_3^- elution during squeezing suggested that more NO_3^- remained in the core (Fig. 4). In retrospect, this finding likely resulted from our tendency to select areas with the strongest mat development when subsampling the relatively small area of sediment required for whole-core squeezing.

Analyses of sheathed *Thioploca* confirmed their high NO_3^- content and also showed a high content of S (Table 3). After subtraction of NO_3^--N, the C_{org} : N ratio was close to the Redfield ratio of 6.6 : 1 (Redfield et al. 1963). Most dramatically, the S content, after subtraction of SO_4^{2-} from sea salt, was ~50% of C_{org} by mass. This high S content may be attributed to S^0 granules contained in the *Thioploca* filaments (Gallardo 1977; Maier and Gallardo 1984*a*).

Mn and Fe—The presence of reactive Mn oxides was only indicated as an enrichment of extractable Mn at the sediment surface (e.g. Aller 1980, 1994; Canfield et al. 1993*b*) at station C41 (Fig. 6), whereas concentrations of

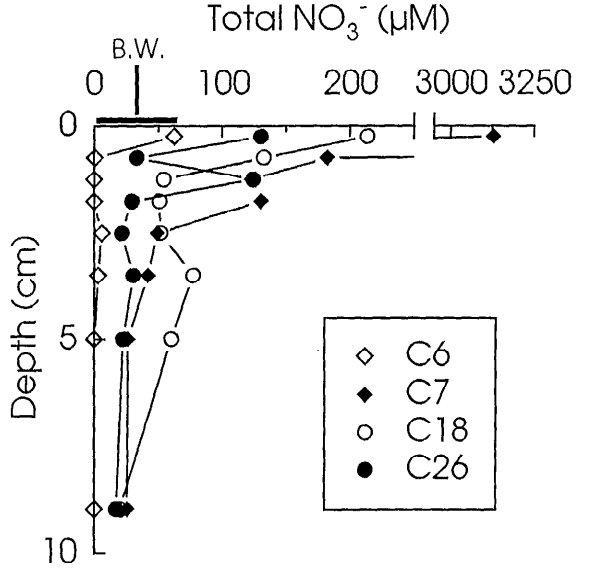

Fig. 5. Depth distributions of initial extractable NO_3^- in sediments used for incubations. The extracted amounts have been converted to equivalent pore-water concentrations. The bar marked B. W. indicates the range of bottom-water NO_3^- concentrations at the shelf stations.

Table 3. Composition of *Thioploca* sample.

	Content (% dry wt)	C_{org} : X (mol : mol)
C_{org}	12.5	1.0
N_{total}	2.53	5.8
NO_3^--N	0.61	24
Residue	1.92	7.6
S_{total}	6.62	5.1
SO_4^{2-}-S	0.84	40
Residue	5.78	5.8
Sea salt	32.2	

Mn were low (<1 μmol g^{-1}) and stable with depth at all other stations (data not shown). The minimal importance of Mn oxides as electron acceptor was further indicated by only small enrichments of pore-water Mn^{2+} to <2 μM in the surface sediment, except at C41, where a maximum of 9 μM was reached at 0.5–1-cm depth (Fig. 6).

The contribution to the oxalate-extractable Fe fraction from Fe(III) decreased with depth and with a concomitant increase in Fe(II), thus demonstrating Fe reduction, except at C6, where the Fe(III) fraction increased slightly with depth (Fig. 7). At the deep stations, all oxalate-extractable Fe was found as Fe(II) at depth, whereas stable positive Fe(III) concentrations were approached at the shallower sites. Because the Fe(III) at C6 was measured in the presence of free H_2S (Fig. 3), it was clearly of low reactivity, which seemed to be the case for the low "background" Fe(III) concentrations reached at the other shelf stations as well. This result was confirmed by analysis of sediment at the end of the prolonged incubations at C7 and C18. Although H_2S accumulated to millimolar levels during these incubations (*see below*), the Fe(III) concentrations did not change in the deeper intervals. At the surface, the Fe(III) fraction decreased to near the background value (data not shown). When we take the Fe(III) levels reached at depth in the shelf sediments as an unreactive background, poorly crystalline Fe(III) was available for Fe reduction near the surface at all stations except C6, and the penetration depth of Fe(III) increased offshore, reaching 4–5 cm at C41. The pool sizes of the poorly crystalline Fe(III) and reactive Mn were calculated by subtraction of the unreactive background, taken as the mean concentration at 6–10-cm depth (Table 4).

We did not find an unreactive Fe(III) background at C40 and C41, which implies a better selectivity of the oxalate extraction toward poorly crystalline Fe phases at these stations. This result was likely due to interference from residual Fe(II) in the shelf sediments. For the determination of oxalate-extractable Fe, the sediments were oxidized by air-drying to remove interferences from Fe(II) (*see methods*). This process decreased the Fe yield significantly relative to the extraction of Fe from fresh sediment (data not shown), but we speculate that some Fe(II) remained in the very FeS-rich shelf sediments and catalyzed dissolution of crystalline Fe oxides.

The dithionite (DCA) extraction typically yielded 1.5–2 times as much Fe as did the oxalate extraction, and the excess Fe extracted by DCA only showed small changes with depth (data not shown). This result indicated that a large pool of crystalline Fe oxides of low reactivity was present in all the profiles studied.

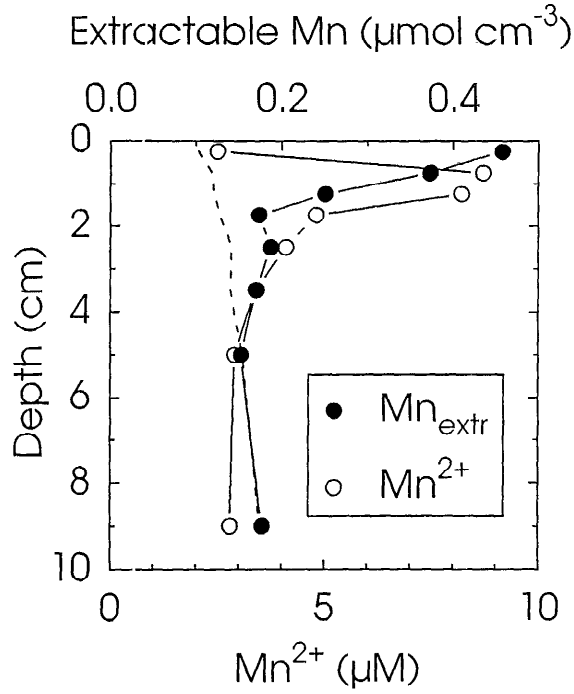

Fig. 6. Depth distributions of extractable and dissolved Mn^{2+} at station C41. Note separate axes. The stippled line shows the unreactive extractable Mn fraction determined from the deepest sections. This fraction decreases toward the surface owing to increasing porosity.

Subsurface maxima of dissolved Fe^{2+} from Fe reduction were in close accordance with the distribution of poorly crystalline Fe(III) (Fig. 3). Thus, C6, which lacked such Fe(III), had only a small Fe^{2+} peak at the surface, whereas stations C7–C26 exhibited sharp Fe^{2+} gradients to ~2-cm depth. At C41, which had the deepest poorly crystalline Fe(III) pool, Fe^{2+} first accumulated at 1-cm depth and reached its maximum at 5-cm depth. The amount of dissolved Fe^{2+}, however, was insignificant in comparison with the Fe(II) pool extracted in oxalate (Fig. 7). This procedure dissolves FeS but not FeS_2, and at the shallowest stations FeS made up a large fraction of this Fe(II) pool (cf. Figs. 7 and 8). At the other sites, however, most of this Fe(II) was not S-bound, and on the slope, non-S-bound Fe(II) was the largest Fe(II) pool measured, exceeding FeS_2 by 5-fold. A large authigenic non-S-bound Fe(II) pool has been measured in other coastal sediments,

Table 4. Pools of reactive Mn and poorly crystalline Fe(III) (mmol m^{-2}) (nd—not detected).

	C6	C7	C18	C26	C40	C41
Mn	nd	nd	nd	nd	nd	4.7
Fe(III)	nd	152	131	67	390	769

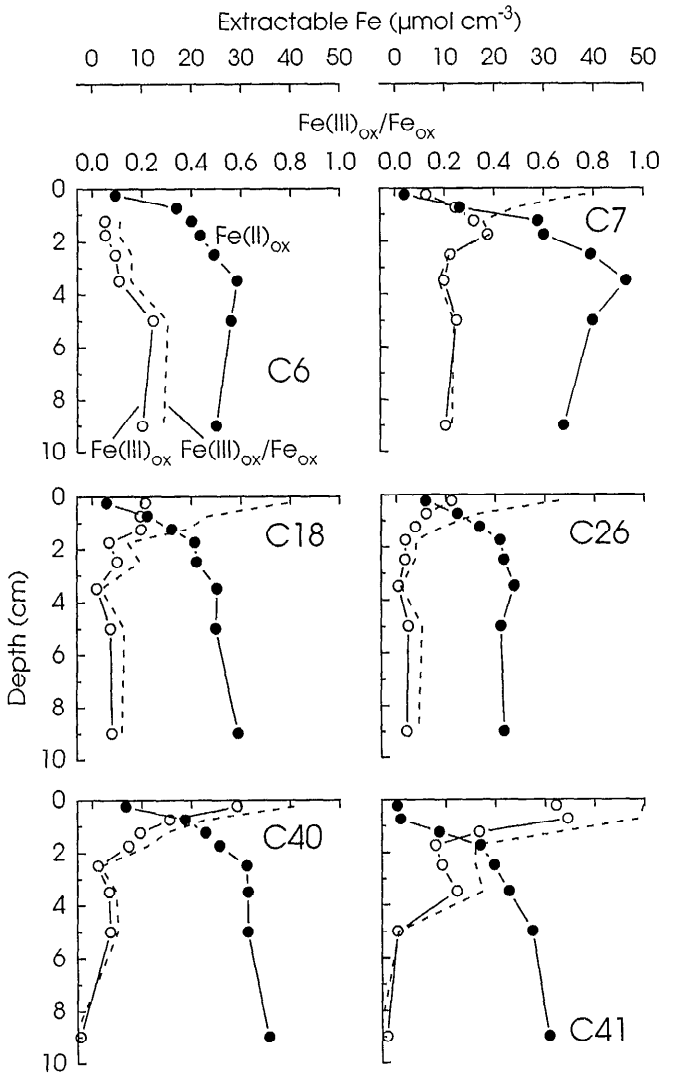

Fig. 7. Depth distributions of oxalate-extractable Fe(II) (●) and Fe(III) (○), and the ratio of oxalate-extractable Fe(III) to total oxalate-extractable Fe (– – –). Note separate scales. Slightly negative concentrations that occurs as $Fe(III)_{ox}$ are found by subtraction of two large numbers.

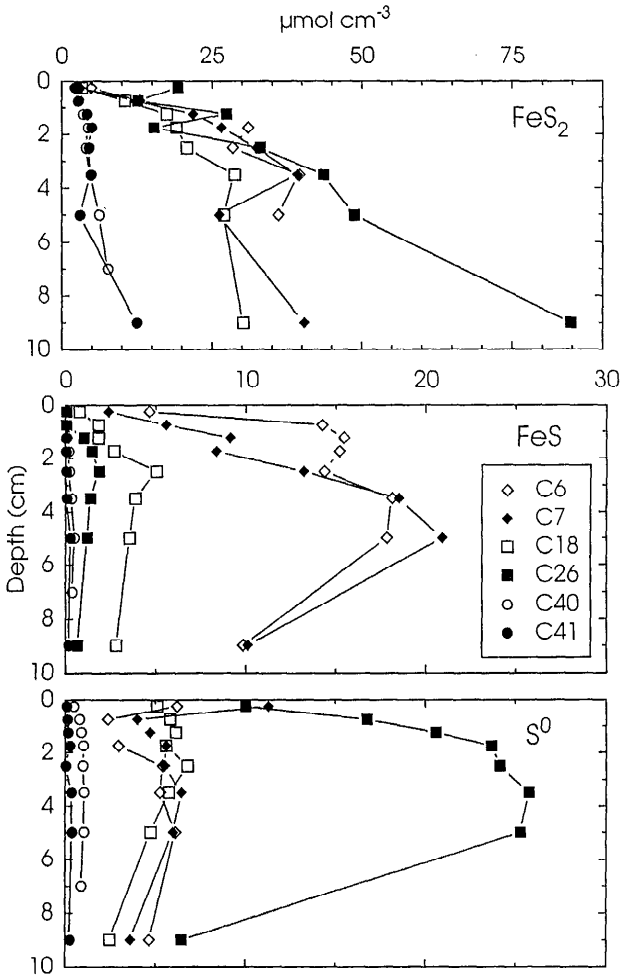

Fig. 8. Depth distributions of reduced sulfur compounds. Note separate scales for FeS_2 and FeS and S^0.

but it is not clear which phases this pool represents (Canfield et al. 1993*b*; Thamdrup et al. 1994*a*).

Sulfur—The pore-water concentration of SO_4^{2-} showed no gradient to 10-cm depth at the slope stations or at C26. At C6, SO_4^{2-} decreased from the seawater level of 28 mM at the surface to 24 mM at 10-cm depth, whereas at C7 and C18 smaller decreases of ~1 mM were observed over this interval (data not shown). High concentrations of H_2S were seen only at C6 (Fig. 3). One core from C18 showed a small H_2S peak of 6 μM near the surface, while the concentrations in another core and in the initial samples from the bag incubations (*see below*) were ≤1 μM. At the other stations, H_2S was not detected (<1 μM). Solid-phase reduced S accumulated at all stations, with pyrite (FeS_2) as the dominating form. Proceeding from the inner shelf to the slope stations, the concentrations of all solid-phase S species decreased markedly. Particularly high levels of FeS were found from the surface at C6 and C7, while a subsurface peak of S^0 was observed at C26.

Incubation experiments: Rates of mineralization—Herein we present results from our bag incubations, including total rates of C mineralization and the contributions of the individual e^- acceptors to this process. The increases in concentrations of both ΣCO_2 and NH_4^+ measured during the short-term sediment incubations were generally linear and showed no systematic deviation from linearity at any station (C7 and C41 shown in Fig. 9). Extended incubations of sediment from C7 and C18 showed that ΣCO_2 and NH_4^+ accumulation rates were stable over a period several times longer than that used for the rate determinations (Fig. 10). Only the surface section from C18 showed a gradual decrease in ΣCO_2 accumulation rates during the 10-d incubation.

Both maximum and depth-integrated rates of ΣCO_2 and NH_4^+ accumulation were extremely high at the shelf

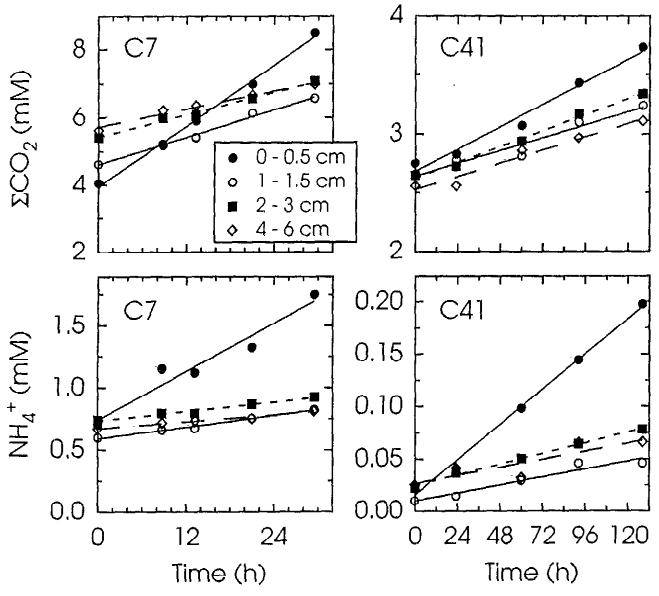

Fig. 9. Examples of ΣCO_2 and NH_4^+ concentration changes during the short-term incubations of sediment from the sites with the highest (C7) and lowest (C41) activities. Note different time and concentration scales.

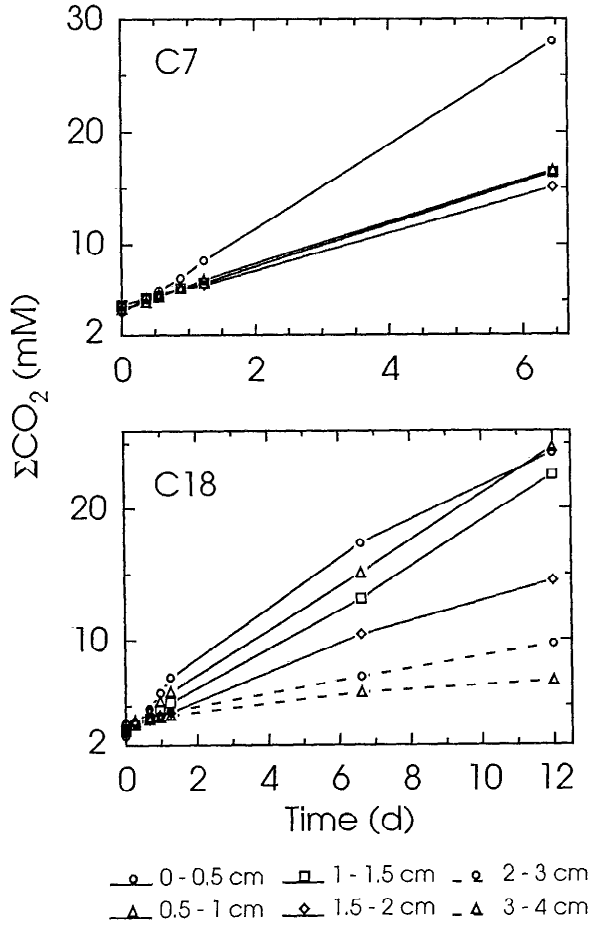

Fig. 10. Changes in ΣCO_2 concentrations during the prolonged incubations of sediment from C7 and C18.

Table 5. Depth-integrated accumulation and SO_4^{2-} reduction rates (mmol m^{-2} d^{-1}) at 0–10-cm depth (0–8 cm at C40).

	Accumulation*		SO_4^{2-} reduction†
	ΣCO_2	NH_4^+	
C6	95.7	9.4	42.5
C7	107±3	14.1±0.8	55.9
C18	56.3±1.3	7.8±0.5	32.8±3.7
C26	50.3±1.9	6.8±0.3	29.9±6.0
C40	11.6±0.6	1.11±0.04	4.80±0.69
C41	9.2±0.4	0.81±0.07	2.66±0.46

* ±SE from linear regression.
† Mean ± half the span from depth-integration of maxima and minima of duplicates. Single determinations at C6 and C7.

stations and decreased 10-fold offshore (Fig. 11, Table 5). There was a close covariation between ΣCO_2 and NH_4^+ accumulation rates at all sites. The ratio of ΣCO_2 accumulation to NH_4^+ accumulation showed no systematic depth variation, but mean values increased from ~8 on the shelf to 11–12 on the slope (Table 6). Ammonium adsorbs to sediment particles (Rosenfeld 1979), and the rate of NH_4^+ accumulation in the pore water consequently underestimates the rate of NH_4^+ production from organic decomposition. The rate of NH_4^+ production can be estimated from the relation (Berner 1980)

$$\text{Rate}(NH_4^+ \text{ production}) = \text{Rate}(NH_4^+ \text{ accumulation}) \times (1 + K),$$

where K is the dimensionless adsorption coefficient with a typical value of 1.3±0.1 in coastal sediments (Mackin and Aller 1984). When this value is used, the average ratios of ΣCO_2 to NH_4^+ accumulation in Table 6 correspond to ΣCO_2 to NH_4^+ production ratios of 3.4 (C18) to 5.2 (C41), provided that ΣCO_2 accumulation was unaffected by the dissolution or precipitation of carbonates.

Calcium carbonate is probably the most significant factor to consider with respect to interference from carbonate dissolution or precipitation. Also, significant precipitation of the relatively minor carbonate francolite (carbonate fluoroapatite; Froelich et al. 1988) was excluded through measurements of dissolved F^- during the incubations. To constrain $CaCO_3$ dissolution or precipitation,

Table 6. $\Sigma CO_2 : NH_4^+$ accumulation ratios in sediment incubations (mol : mol).

Depth (cm)	C7	C18	C26	C40	C41
0–0.5	4.6	7.1	16.0	8.5	5.7
0.5–1	6.9	5.8	11.5	10.6	8.9
1–1.5	8.7	7.1	7.8	15.9	14.4
1.5–2	9.1	7.3	8.4	16.9	8.0
2–3	8.8	8.6	4.9	14.1	13.2
3–4	7.7	4.6	7.2	6.7	11.4
4–6	9.8	13.2	6.6	13.2	14.7
8–10*	9.1	9.6	7.3	10.5	13.1
Mean	8.1	7.9	8.7	12.1	11.2

* At C40, 6–8-cm depth.

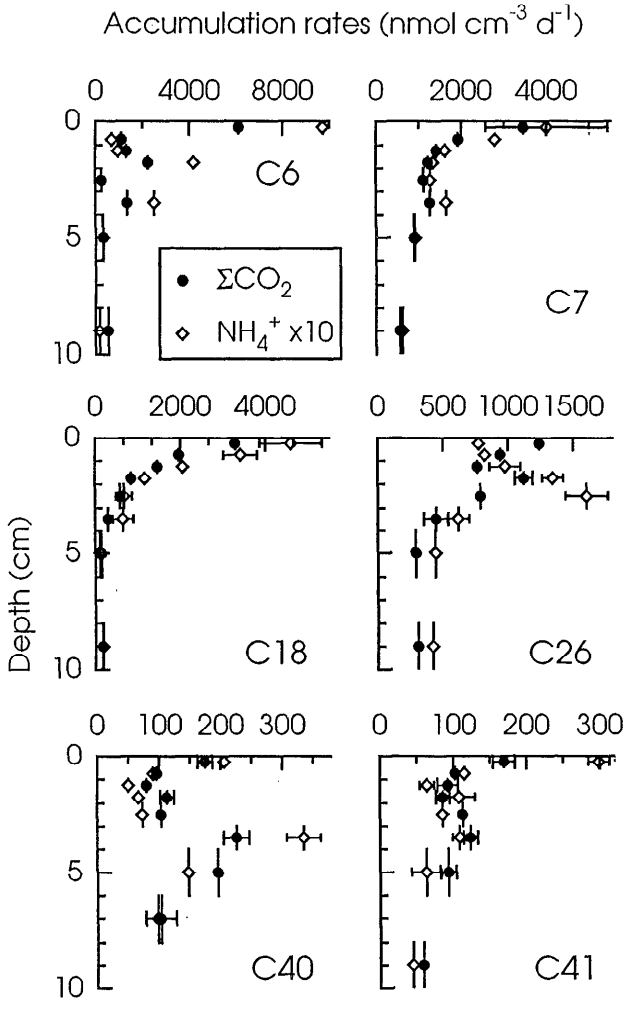

Fig. 11. Depth distributions of ΣCO_2 and NH_4^+ accumulation rates ±SE at all stations. Note that rates for NH_4^+ have been multiplied by 10. Errors could not be calculated for C6.

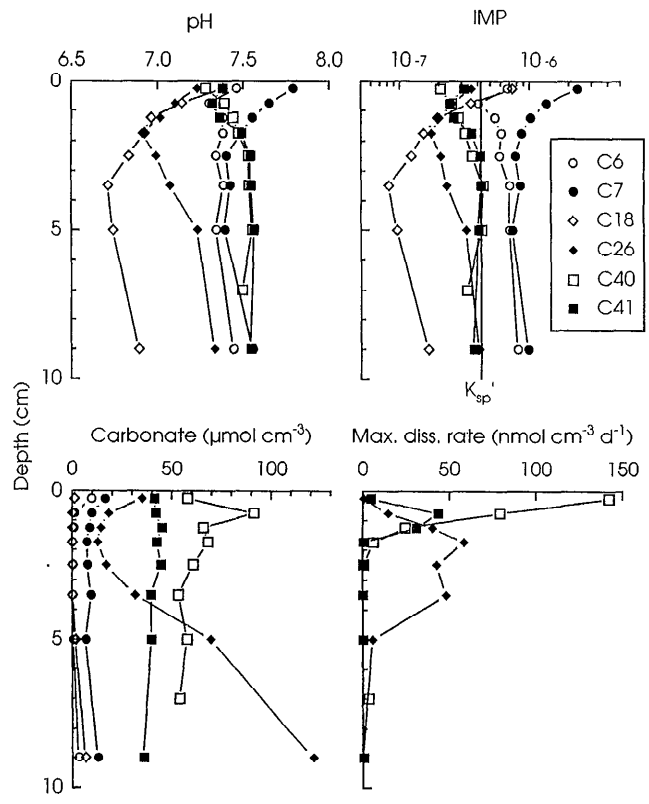

Fig. 12. Depth distributions of parameters used in carbonate dissolution rate calculations. pH was measured at the end of the short-term incubations. For ion molality products (IMP, *see text*), the vertical line represents the apparent solubility constant of calcite. Dissolution rates were calculated assuming k of 5% d^{-1} (Eq. 1).

ion molality products (IMP) were first calculated from Ca^{2+} and ΣCO_2 concentrations and pH and then compared to the apparent solubility constant, K_{sp}', of calcite (Mucci 1983), which in the form of foraminiferal tests was found to be the main contributor to the low carbonate content of the sediments (Fig. 12). Carbonic acid dissociation constants in seawater at 34.5‰ S and 11.5°C (shelf sites) or 5°C (slope sites) were used (Mehrbach et al. 1973). Concentrations of pore-water Ca^{2+} did not deviate significantly from the bottom-water level (data not shown). Pore waters at C7 were supersaturated with respect to calcite, whereas clear undersaturation was observed at C18 and C26 and near the surface at C40 and C41. Measurements of dissolved Ca^{2+}, however, indicated no change during any of the incubations to levels exceeding the precision of the Ca^{2+} determination (data not shown). Given this precision, ΣCO_2 changes owing to $CaCO_3$ precipitation or dissolution were limited to <70 and <30 nmol cm^{-3} d^{-1} during the prolonged incubations at C7 and C18. Because ΣCO_2 accumulation rates at C7 and C18 (Fig. 11) were much higher than these values, we immediately excluded a significant contribution from $CaCO_3$ precipitation or dissolution to the C accumulation rates for these stations. At the remaining stations, the shorter incubation times made the potential precipitation or dissolution rates correspondingly larger (i.e. 250, 110, and 80 nmol cm^{-3} d^{-1} at C26, C40, and C41, respectively).

To further constrain calcite dissolution rates at the outer stations that experienced undersaturation, we applied a normal rate law expression with dissolution rate as a function of $CaCO_3$ content and degree of undersaturation:

$$\frac{dCa^{2+}}{dt} = C_{CaCO_3} \times k \times \left(1 - \frac{IMP}{K_{sp}'}\right)^n. \quad (1)$$

k is a rate constant, C_{CaCO_3} is the carbonate content, and n equals 4.5 for calcite (Morse 1978; Keir 1980). For the undersaturated surface intervals at C40 and C41, dissolution rates similar to the measured ΣCO_2 accumulation rates (Fig. 11) may be generated by using k of 5% d^{-1} (Fig. 12). At this value of k, $CaCO_3$ dissolution could only contribute to the measured ΣCO_2 accumulation above 1.5-cm depth. However, significant $CaCO_3$ dissolution in the surface sediments should increase the accumulation ratios of ΣCO_2 to NH_4^+ to higher values than in the deeper

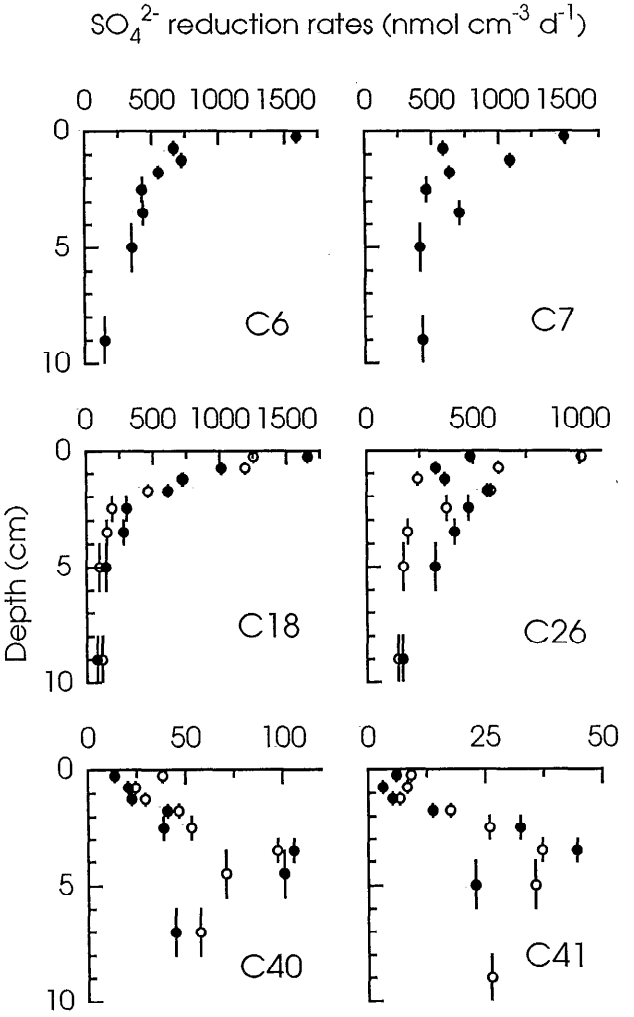

Fig. 13. Depth distributions of SO_4^{2-} reduction rates from all stations (●—first determination; ○—second determination; only one determination was made at C6 and C7).

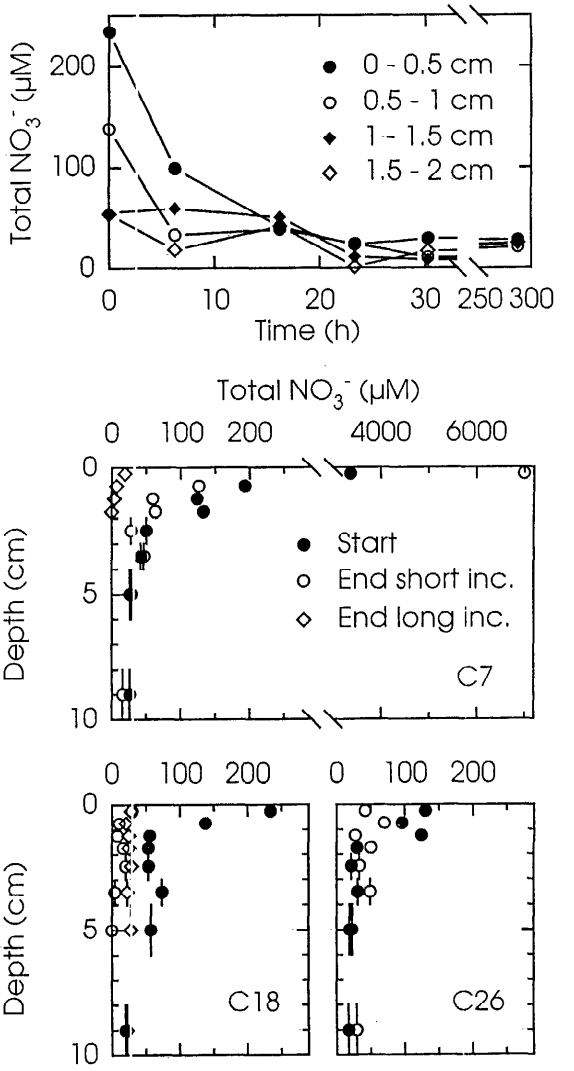

Fig. 14. Changes in extractable NO_3^- concentrations during sediment incubations. Top: Time course from short-term (0–30 h) and prolonged (to 300 h) incubations of four depth intervals at C18. Center and bottom: Depth distributions at the beginning and end of the short-term incubations as well as at the end of the prolonged incubations (C7, 0–2 cm and C18 only).

layers, where dissolution cannot occur. By contrast, the observed $\Sigma CO_2 : NH_4^+$ ratios increase with depth (Table 6). The same is the case at C26, where the potential dissolution rates increase from the surface while $\Sigma CO_2 : NH_4^+$ accumulation ratios decrease. Also, a comparison between stations does not support significant $CaCO_3$ dissolution rates, because $\Sigma CO_2 : NH_4^+$ accumulation ratios in zones where dissolution could be significant are comparable to zones where dissolution has been excluded. From these considerations, we conclude that the ΣCO_2 accumulation rates represent C oxidation and may be only marginally affected by dissolution or precipitation.

Table 7. Molar ratio of ΣCO_2 production to SO_4^{2-} consumption during prolonged incubations.

Depth (cm)	C7	C18
0–0.5	2.21	1.98
0.5–1	1.89	1.93
1–1.5	1.59	1.93
1.5–2	2.42	1.67
Mean±SD:	1.95±0.26	

Sulfate reduction—Rates of SO_4^{2-} reduction measured by means of the radio tracer technique resembled rates of C mineralization (i.e. extreme surface rates and exponential decreases with depth on the shelf, as well as lower rates downslope; Fig. 13). In contrast to the C mineralization rates, however, surface rates of SO_4^{2-} reduction at C40 and C41 were low, with pronounced subsurface maxima at 3–4 cm. At the slope sites and at C18, little variability was observed between the two SO_4^{2-} reduction rate determinations, whereas larger but unsystematic variation was observed at C26 (Table 5, Fig. 13).

The mean ratio of ΣCO_2 production to SO_4^{2-}, depletion

Table 8. Mean NO_3^- consumption rates (nmol cm^{-3} d^{-1}) during bag incubations (nd—not detected).

Depth (cm)	C7	C18	C26
0–0.5	450*	158	55
0.5–1	38	85	19
1–1.5	45	22	58
1.5–2	47	20	13
2–3	15	18	nd
3–4	nd	36	nd
4–6	nd	21	nd
8–10	nd	nd	nd
Σ, mmol m^{-2} d^{-1}	3.1	2.6	0.7

* Mean rate over entire incubation (*see text*).

during the prolonged incubations was close to 2.0 (Table 7). The uppermost interval at C7 was an exception, as a large NO_3^- pool persisted throughout the short-term incubation and could have contributed to C oxidation or reoxidation of H_2S during the prolonged incubation (*see below*). This pool may explain the higher $\Delta\Sigma CO_2 : \Delta SO_4^{2-}$ ratio observed there. Otherwise, the larger deviations from the mean ratio were found in the incubations with the smallest concentration changes and, hence, the largest associated errors.

During the short-term incubations, H_2S was detected only at C6 and at 8–10-cm depth at C7, where it rose from below detection to 64 μM in 30 h. In the prolonged incubation of C7 and C18 sediments, however, H_2S accumulated rapidly in the upper sections, with maximum concentrations reaching 4.5 and 3.0 mM at the surface of C7 and C18, respectively. An even larger increase was observed in acid-volatile sulfide (AVS = H_2S + FeS; data not shown), and FeS precipitation was seen as a blackening of the sediments.

Other C oxidation pathways—Although both O_2 and NO_3^- persisted to 5–10 mm in the pore waters at C40 and C41, their presence was dependent on a continuous supply from the bottom water. Because the sediment was sectioned for the incubation experiments, this supply was cut off, and the small standing stocks of the two species were rapidly depleted at the beginning of the incubations (data not shown). At the anoxic shelf sites, total sediment NO_3^- contents generally decreased during the incubations (Fig. 14) (the time course from C18 is given as an example). As discussed above, most of the NO_3^- was present within the *Thioploca,* and the stable background level of about 20 μM is assumed to be an artifact from the extraction. The overall highest NO_3^- contents were measured at 0–0.5-cm depth at C7, and this short-term incubation alone showed an increase in NO_3^-. Because NO_3^- production is not likely during the anoxic incubation, we expect this result to be due to the presence of NO_3^--rich *Thioploca* bundle(s) in the subsample taken from the bag after the short-term incubation. At the end of the prolonged incubation, NO_3^- was depleted to the background level at this depth too.

Average rates of NO_3^- consumption during the short-term incubations are given in Table 8. For 0–0.5-cm depth at C7, the rate has been estimated by means of the initial concentration and the NO_3^- depletion observed at the end of the prolonged incubation. The time course of NO_3^- consumption for C18 (Fig. 14) showed that rates were not constant but decreased as the background level was approached. The average rates may therefore underestimate the initial rates and thereby presumably also the in situ NO_3^- consumption.

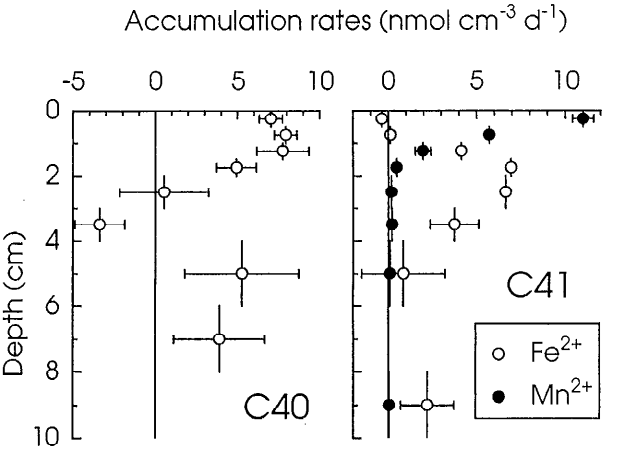

Fig. 15. Depth distributions of accumulation rates ±SE of dissolved Fe^{2+} and Mn^{2+} during sediment incubations. At C40, no Mn^{2+} accumulated.

Pore-water Mn^{2+} accumulated steadily at C41 between 0 and 1-cm depth (Fig. 15), in accordance with the distribution of reactive Mn oxides (Fig. 6), whereas the concentration remained <4 μM for all other incubations at all other stations. Also, at C41 significant buildup of dissolved Fe^{2+} was observed throughout the incubation in the sections from 1- to 4-cm depth, and at C40 from 0 to 2 cm (Fig. 15). Deeper in these sediments, the changes in Fe^{2+} were too small relative to the high initial concentrations for liberation to be detected with certainty. At all the shelf sites, Fe^{2+} in the pore water increased only at 0–0.5 cm (data not shown). In deeper sections, the Fe^{2+} concentration was constant or decreased owing to precipitation of solid Fe(II).

Discussion

Rates of C oxidation—By measuring the accumulation of ΣCO_2, we have directly quantified the rates and depth distribution of carbon mineralization in the sediments. A significant influence from carbonate dissolution or precipitation could be excluded at all of these metabolically active sites. Würgler bags provided a convenient setup for repeated pore-water sampling and thereby for determination of accurate C oxidation rates. We kept incubations brief so that the original metabolic pathways and sediment microbial populations were maintained as well as possible. Accumulation rates of ΣCO_2 and NH_4^+ were therefore stable throughout the short-term incubations (Fig. 9) and were even quite stable when incubations were

continued much longer (Fig. 10). In situ measurements of ΣCO_2 fluxes from the shelf sediments (R. N. Glud et al. in prep.) showed a considerable local variability, but the range of flux rates corroborates the range of depth-integrated C oxidation rates from the bag incubations (Table 5). Further evidence that the sectioning and homogenization of sediment necessary for the incubations did not lead to major immediate changes in the turnover rates was that both the depth-integrated and the maximal SO_4^{2-} reduction rates agreed well with those obtained with the whole-core injection technique during the same cruise (Jørgensen 1978; T. G. Ferdelman et al. in prep.). Canfield et al. (1993*a*) found that depth-integrated C oxidation rates in their bag incubations were about twice as high as rates determined from flux measurements, but they suggested that this could result from too high temperature during incubation and sediment handling or from decay of entombed fauna. Our results do not indicate a similar strong stimulation of C mineralization during the incubations, and hence we take the rates as estimates of the in situ sediment metabolism.

The rates of C oxidation in sediments of the Chilean margin (Fig. 11) ranged from high to extreme. The maxima are an order of magnitude higher than those found in sediments of the Norwegian Trough (Canfield et al. 1993*b*) or the Amazon shelf (Aller et al. 1996). The depth-integrated rates from the shelf (Table 5) are the highest reported from open waters (cf. Henrichs 1992; Canfield 1993) and are similar to results from small coastal embayments with very rapid sediment accumulation, such as Cape Lookout Bight, North Carolina (Martens and Klump 1984). Also, the SO_4^{2-} reduction rates from the shelf sites (Table 5) were similar to those in Cape Lookout Bight (Crill and Martens 1987) and the maxima approached those measured in solar pond-microbial mats (Jørgensen and Cohen 1977; Canfield and Des Marais 1991). The extreme activity is further demonstrated by comparison to SO_4^{2-} reduction rates in sediments from the Peru upwelling region, which is also covered with *Thioploca*. There, Fossing (1990) measured rates of 4–26 mmol m^{-2} d^{-1} to 20-cm depth with maxima up to 300 nmol cm^{-3} d^{-1} (i.e. 5 times lower than those presented here).

Although eutrophic conditions with mass mortality of fauna were observed 100 yr ago in Concepción Bay (Ahumada et al. 1983), stations at the mouth of the Bay (C6 and C7) could presently be affected by further eutrophication from the town of Talcahuano. The continued intense C oxidation offshore at C18 and C26, however, could only be sustained by extreme primary productivity owing to upwelling. High productivity was obvious from both the O_2 depletion in the water column and from direct measurements during the cruise that showed total primary productivities over the shelf of ~10 g C m^{-2} d^{-1} (O. Ulloa pers. comm.) and the productivity supports an intense (human and avian) fishery in the region.

Variations in C oxidation rates were only weakly reflected in the C_{org} content of the sediments (Figs. 2, 11). The turnover times for C_{org} (concn/oxidation rate) in the surface mat at C7 and C18 were extremely short, 0.22 and 0.41 yr, respectively, which corresponds to rate constants of 4.5 and 2.4 yr^{-1}, assuming first-order decay of C_{org}. These constants approach those of fresh plankton (Westrich and Berner 1984), which implies a close coupling of benthic C oxidation and production in the water column. The turnover time for C_{org} increased dramatically both with sediment depth, reaching 4.9 and 12 yr at 8–10-cm depth at C7 and C18, and with water depth, reaching 13 and 57 yr in the top and bottom sections at C41, respectively. The large variation in reactivity was not due to differences in C oxidation pathways, because SO_4^{2-} reduction was the dominating respiration at all depths at the shelf stations as well as at the deepest section of C41 (*see below*). The varying reactivities of C_{org} were only weakly reflected in the C_{org} : N ratios (Fig. 2) and in the ΣCO_2 : NH_4^+ accumulation ratios (Table 6).

Although the reactivity of C_{org} decreased offshore, the rates of decomposition at 1,000- and 2,000-m depth were still high and within the range of many shelf sediments (Devol and Christensen 1993; Canfield 1993; Canfield et al. 1993*a*). The depth dependence of C oxidation rates (COR) was fit closely by the power function

$$COR_{total} = 54.4 \text{ mmol } m^{-2} d^{-1} \times (z/100)^{-0.60\pm0.07} \quad (R = 0.991).$$

z is water depth in meters. Devol and Christensen (1993) fitted a similar function to C oxidation rates in Washington state continental margin sediments and found an exponential factor of -0.91 ± 0.10, implying much stronger attenuation of the rates with depth. Thus, our measured COR at 2,000 m was 2.5 times higher than that predicted by their coefficient.

Pathways of C mineralization—The oxidation of organic matter in the sea floor proceeds through a chain of biologically catalyzed processes, including hydrolysis, fermentation, and respiration. Under anoxic conditions, the production of ΣCO_2 is not necessarily entirely coupled to respiration since some ΣCO_2 may be released during fermentation with concomitant production of reduced substances such as ethanol or H_2 (e.g. Schink 1988). Because these fermentation products are favorable substrates for anaerobic respiratory bacteria, they are kept at low concentrations by rapid consumption (Sørensen et al. 1981; Parkes et al. 1989) and, overall, the oxidation of C is balanced by the reduction of the inorganic oxidants O_2, NO_3^-, oxides of Mn and Fe, and SO_4^{2-} (*see also* Westrich 1983). In addition to the oxidative pathways of C mineralization, net ΣCO_2 production in sediments may result from methanogenesis, which does not represent a net C oxidation. Generally, however, SO_4^{2-}-reducing bacteria outcompete methanogens for common substrates so that methanogenesis only becomes significant deeper in marine sediments, where SO_4^{2-} is depleted (e.g. Martens and Klump 1984). We therefore did not expect this process to affect our ΣCO_2 measurements, which was confirmed by direct measurements of methanogenesis at stations C7 and C18 that showed rates $<1‰$ of ΣCO_2 production (T. G. Ferdelman et al. in prep.).

The ΣCO_2 production associated with SO_4^{2-} reduction can be calculated from the SO_4^{2-} reduction rates and the overall stoichiometry of C_{org} oxidation with SO_4^{2-}. In

conversions of oxidant consumption to C oxidation in marine sediments, an oxidation state of 0, as for carbohydrates, is commonly used for the C being oxidized (e.g. Froelich et al. 1979; Reimers et al. 1992; Canfield et al. 1993*a*). For SO_4^{2-} reduction, this corresponds to the reaction

$$2CH_2O + SO_4^{2-} \rightarrow 2HCO_3^- + H_2S. \quad (2)$$

The use of this stoichiometry is supported by the mean ratio of ΣCO_2 production to SO_4^{2-} depletion of 2.0 : 1 measured during the prolonged incubations, where H_2S accumulation signaled the depletion of reactive Fe phases (Canfield et al. 1992) and SO_4^{2-} reduction could thus be assumed to be the only process contributing to C oxidation (Table 7). We have used this ratio to calculate ΣCO_2 production from the SO_4^{2-} reduction rates of the short-term incubations. The use of a 2.0 : 1 ratio is also supported by studies in Long Island Sound sediments (Westrich 1983) and sapropels from Bermuda (Boudreau et al. 1992), whereas a $\Sigma CO_2 : SO_4^{2-}$ ratio of 1.7 : 1 has been reported for SO_4^{2-} reduction in Cape Lookout Bight sediment (Alperin et al. 1994). A recent global estimate of the $C_{org} : O_2$ reaction ratio in pelagic remineralization (Anderson and Sarmiento 1994) corresponded to a C_{org} oxidation state of −0.7, which also translates to a $C_{org} : SO_4^{2-}$ ratio of 1.7 : 1. This ratio would correspond to a 15% lower contribution of SO_4^{2-} reduction to C oxidation than would the measured value of 2.0 : 1.

The importance of SO_4^{2-} reduction and, by difference, of other e^- acceptors in total C oxidation can be determined by comparing COR_{total} to the calculated C oxidation by SO_4^{2-} reduction ($COR_{sulfate}$; Fig. 16). At C41, the large excess ΣCO_2 production in the surface intervals indicates that e^- acceptors other than SO_4^{2-} were important at this site (Fig. 16). The excess decreased with depth, and by 8–10 cm, SO_4^{2-} reduction accounted for all ΣCO_2 accumulation. At C40, $COR_{sulfate}$ was relatively more important, and at all the shelf sites, $COR_{sulfate}$ was close to COR_{total} at all depths. To further deduce the relative importance of the C oxidation pathways, we followed a scheme similar to that introduced by Canfield et al. (1993*b*), as summarized in Table 9. The slope and shelf stations are discussed separately since the mass occurrence of *Thioploca* at the shelf stations requires special considerations.

Slope stations—The depth intervals where oxic respiration and denitrification could be of importance are identified from the distributions of O_2 and NO_3^-. At the slope stations C40 and C41, with the limitation of the 0.5-cm depth resolution of our bag incubations, these intervals included 0–1-cm depth (Fig. 3). At C41, redox cycling of Mn in this interval was demonstrated both by the depth distributions of Mn species (Fig. 6) and by the accumulation of Mn^{2+} during incubations (Fig. 15). At both sites, sulfate reduction was observed in the surface sections, and at C40, Fe^{2+} also accumulated (Figs. 13, 15). The depletion of O_2 and NO_3^- during incubation, however, likely stimulated reduction of Mn, Fe, and SO_4^{2-}. Previous studies of sediments with similar chemical zonation have concluded that Mn reduction was mainly

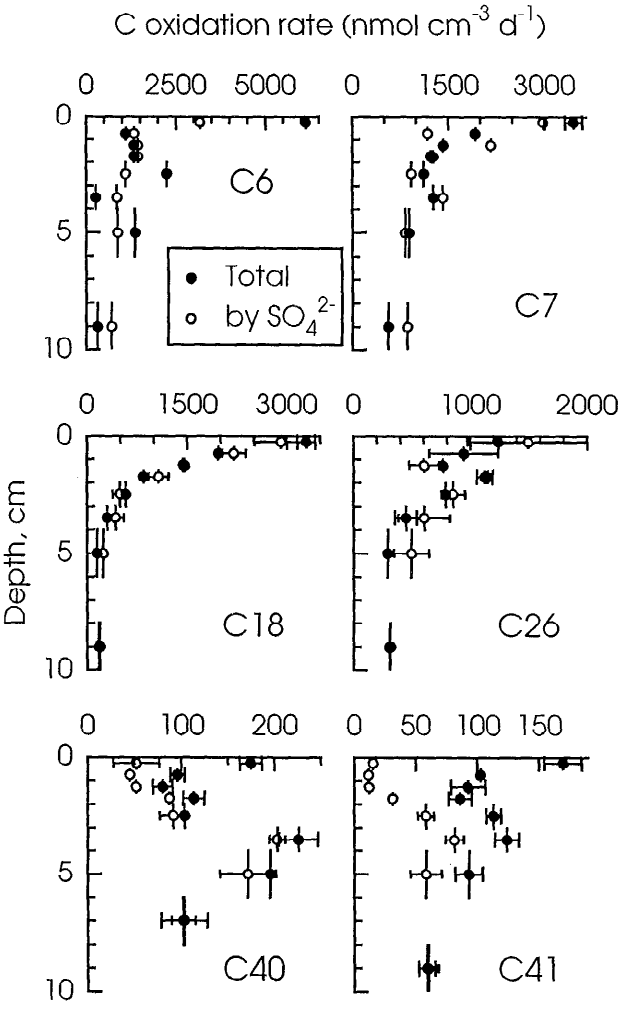

Fig. 16. Comparison of total observed carbon oxidation rates (±SE) to C oxidation due to SO_4^{2-} reduction (error bars span duplicate determinations). No errors were calculated for C6 or SO_4^{2-} reduction rates at C7.

associated with the reoxidation of reduced Fe and S (Canfield et al. 1993*b*; Aller 1994; Thamdrup et al. 1994*a*). This could also be the case at C41, where rapid reoxidation of Fe^{2+} with Mn oxides (Postma 1985) may have masked Fe reduction. The low levels of Mn encountered throughout the transect probably resulted from Mn mobilization from the sediments underlying O_2-depleted bottom water (Thamdrup et al. 1994*b*). From these considerations it follows that the pathways of C oxidation in the surface interval cannot be individually quantified.

Of the total C oxidation, the 0–1-cm interval accounted for 12% at C40 and 15% at C41 (Fig. 11), and we tentatively use these values as estimates of the combined contribution of oxic respiration, denitrification, and, at C41, dissimilatory Mn reduction to mineralization (Table 10). This rests on the assumption, also made by Canfield et al. (1993*a*), that the total C oxidation rate was not affected by the depletion of O_2 and NO_3^-. This assumption is supported by the observation that relatively fresh organic matter appears to decay at approximately similar rates under oxic and anoxic (SO_4^{2-}-reducing) conditions,

Table 9. General scheme for deducing pathways of carbon oxidation.

Step	Comment
Depth distribution of ΣCO_2 production	Total C oxidation rates
$CaCO_3$ precipitation/dissolution	Potential correction to C oxidation rates
Depth distribution of NH_4^+ accumulation	Check on C metabolism
O_2 and NO_3^- distributions	Max. depths of oxic respiration and denitrification
Combined C oxidation by O_2 and NO_3^- estimate	ΣCO_2 production in O_2/NO_3^- zone
Combined C oxidation by Mn, Fe, and SO_4^{2-} reduction	ΣCO_2 production below O_2/NO_3^- zone
SO_4^{2-} reduction rates	Direct determination
ΣCO_2 production by SO_4^{2-} reduction	From stoichiometry
Combined C oxidation by Mn and Fe reduction	Difference between total and SO_4^{2-}-coupled C oxidation
Separation of Mn and Fe reduction	From oxide distributions and accumulation of Mn^{2+} and Fe^{2+}

but as mineralization proceeds, the oxic pathway may become relatively faster (cf. Canfield 1993; Kristensen et al. 1995). The efficiency of Mn and Fe reduction in this context has not been specifically investigated, and further investigations are clearly required to test our assumption. To better constrain the contribution from oxic respiration, measurements like the present may be combined with determination of benthic fluxes (Canfield et al. 1993*a*). Unfortunately, such determinations were not available for the slope sites.

While the relative importance of the e^- acceptors near the sediment surface cannot be determined, Fe(III) was the only available oxidant below 1 cm other than SO_4^{2-}. The comparison of total and SO_4^{2-} reduction-coupled C oxidation (Fig. 16) showed a distinct excess C oxidation to 6-cm depth at C41 and to 2 cm at C40, with a slight excess extending to 6 cm. There was close agreement between excess C oxidation, the distribution of poorly crystalline Fe(III) (Fig. 7), and the depths at which dissolved Fe^{2+} accumulated during the incubations (Fig. 15). In the presence of poorly crystalline Fe hydroxides, but not crystalline forms, Fe-reducing bacteria have been shown to outcompete SO_4^{2-}-reducing bacteria for common substrates (Lovley and Phillips 1987). Subtraction of $COR_{sulfate}$ from COR_{total} for intervals below 1-cm depth (Fig. 16) gives excess C oxidation rates that correspond to 12 and 29% of total C oxidation at C40 and C41, respectively (Table 10), or 13 and 34% of the C oxidation in the anoxic portions, which we attribute to Fe reduction. As mentioned above, it is possible that Fe reduction also contributed to C oxidation within the upper 0–1-cm interval, at least at C40, but this contribution cannot be quantified. Although Fe reduction cannot be measured directly, we conclude that this process was significant for C oxidation at both slope sites.

The rates of Fe^{2+} (and Mn^{2+}) accumulation at C40 and C41 were small in comparison to C oxidation rates. Canfield et al. (1993*b*) showed that accumulation rates of pore-water Mn^{2+} and Fe^{2+} strongly underestimate rates of Mn and Fe reduction because of adsorption or precipitation of the reduced species. We did not determine the adsorptive characteristics of the Chilean sediments, but the Fe extractions demonstrate depthwise accumulation of most of the Fe(II) in a solid, nonsulfidic phase (Figs. 7, 8). Owing to the high initial Fe(II) concentrations, it was not possible to quantify changes in the solid phases over the short-term incubations.

The maintenance of high Fe (or Mn) reduction rates depends on continuous mixing of metal oxides and fresh organic matter into the sediments through bioturbation or other mixing processes (Aller 1990; Canfield et al. 1993*b*). Because most Fe(II) is also particle-bound, mixing is also important for its upward transport to allow Fe oxidation at the surface, as demonstrated by the opposed gradients of Fe(II) and Fe(III) (Fig. 7). The relative constancy of both C_{org} and COR_{total} with depth at the slope sites also indicated rapid mixing of organics into the sediments (Figs. 2, 16).

We have no quantitative estimates of the sediment mixing, but ^{210}Pb distributions showed mixing to at least 5-cm depth at C41 and to 4 cm at C40 (M. A. Salamanca pers. comm.). It is thus likely that deeper mixing at C41, in conjunction with lower total C mineralization rates, resulted in a larger contribution from Fe reduction there

Table 10. Rates of carbon oxidation (mmol m^{-2} d^{-1}) and relative importance (%) of carbon oxidation pathways (nd—not detected).

	C6		C7		C18		C26		C40		C41	
Pathway	Rate	%	Rate	%	Rate	%	Rate	%	Rate	%	Rate	%
O_2 resp.	nd		nd		nd		nd		1.4±0.1	12	1.4±0.1	15
NO_3^- red.	nd		nd*		nd*		nd*		nd			
Mn. red	nd		nd		nd		nd					
Fe red.	nd		nd		nd		nd		1.4±1.5	12	2.7±1.0	29
SO_4^{2-} red.	85	89	112	104	66±7	117	60±12	118	9.1±1.4	79	5.2±0.9	56

See text for principles of calculation. Errors have been propagated as SD from those given in Table 5.
* Nitrate consumption was observed (Table 8) but did not appear directly coupled to C oxidation (*see text*).

than at C40. The turnover times of the poorly crystalline Fe(III) pools through Fe reduction were 70 d at C40 and 71 d at C41. These values are similar to those calculated for the Skagerrak sediments, where Fe reduction was very important (70–79 d; Canfield et al. 1993*b*). The surface concentration of oxalate-extractable Fe (Fig. 7) combined with a sediment accumulation rate of 0.15 cm yr^{-1} (M. A. Salamanca pers. comm.) yields a delivery flux of poorly crystalline Fe of 0.14 mmol m^{-2} d^{-1} for both sites. Thus, on average, each Fe atom was reduced and reoxidized (rate of reduction/delivery flux) 31 and 77 times before burial at C40 and C41, respectively.

The calculations above concern only Fe cycling coupled to C oxidation. The absence of H_2S from the pore water, in spite of active SO_4^{2-} reduction (Figs. 3, 13), and the accumulation of iron sulfides, mainly FeS_2 (Fig. 8), indicate additional coupling of the Fe and S cycles. For other coastal sediments, it has been shown that reaction with free Fe(III) oxides may buffer pore-water H_2S below the detection limit in the presence of SO_4^{2-} reduction (Goldhaber and Kaplan 1974; Canfield 1989; Thamdrup et al. 1994*a*). Hydrogen sulfide reacts with Fe oxides by the overall reaction (Pyzik and Sommer 1981)

$$3H_2S + 2FeOOH \rightarrow 2FeS + S^0 + 4H_2O. \quad (3)$$

If all H_2S produced reacted according to this equation, the SO_4^{2-} reduction rates measured at C40 and C41 would correspond to reactions of 3.0 and 1.7 mmol Fe(III) m^{-2} d^{-1}, respectively, which are equivalent to 54 and 16% of the calculated organotrophic Fe reduction (Table 10). Hydrogen sulfide reacts most rapidly with poorly crystalline Fe oxides, but crystalline oxides also react (Canfield 1989; Canfield et al. 1992). A role for crystalline Fe oxides was indicated at the slope sites, where H_2S was not detected to at least 20-cm depth (Fig. 3), far beyond the penetration depth of the poorly crystalline Fe oxides (Fig. 7). Thus, because of the coupling to the S cycle, the turnover of the poorly crystalline Fe(III) pool should be somewhat faster than calculated from C oxidation alone.

Shelf stations—Bottom-water anoxia on the shelf excluded oxic respiration from the sediments. However, this situation represented a seasonal extreme. The cruise took place in late summer, which is when *Thioploca* mats have their widest distribution and the O_2 minimum zone reaches its shallowest depth (V. A. Gallardo pers. comm.). Bottom-water anoxia was documented in several measurements between 12 and 24 March (J. K. Gundersen and R. N. Glud pers. comm.), suggesting that the depletion lasted for up to 2 weeks. Still, juvenile squat lobsters and polychaetes survived at the sediment surface. The *Thioploca*-covered shelf area is the nurseryground of the squat lobster *P. monodon,* and an adaptation to low O_2 levels might reduce predation of the juveniles (Roa et al. 1995). We must therefore assume that absence of O_2 was a transient phenomenon that coincided with the cruise and may be triggered by a pulse of primary production associated with an upwelling event. Hence, our rate measurements were likely close to the summer maximum, and the complete lack of O_2 at the sediment surface was not typical for the area. We cannot speculate on the importance of O_2 in C cycling during times of the year when O_2 is present in high concentrations in the overlying water.

A benthic NO_3^- uptake of 2.1 mmol m^{-2} d^{-1} was measured in situ at C18 during the cruise (Fossing et al. 1995; R. N. Glud et al. in prep.). If we assume denitrification according to

$$5CH_2O + 4NO_3^- \rightarrow 5HCO_3^- + 2N_2 + 2H_2O + H^+, \quad (4)$$

this uptake corresponds to a C oxidation of 2.6 mmol m^{-2} d^{-1}, or <5% of the total C oxidation rate (Table 5). However, determination of the fate of NO_3^- in the shelf sediments and its role in C oxidation is complicated by the large accumulation of NO_3^- in the *Thioploca* filaments. Hence, when $^{15}NO_3^-$ was added to the overlying water, essentially all of it was taken up and stored by the *Thioploca* and was not used immediately for C mineralization (L. P. Nielsen pers. comm.; R. N. Glud et al. in prep.). Thus, we assume that the large NO_3^- pool in the sediments was metabolized by *Thioploca* and that the sediment NO_3^- consumption was not directly coupled to C oxidation, because the organism is presumed to couple NO_3^- reduction to oxidation of H_2S (Fossing et al. 1995).

There was a close match between the measured C oxidation rates and the rates attributable to SO_4^{2-} reduction on the shelf (Fig. 16). A very close match was found at C18; also at C26, the mean $COR_{sulfate}$ agreed well with COR_{total}, although the comparison at C26 was blurred somewhat by the differences between the two SO_4^{2-} reduction rate determinations. The single $COR_{sulfate}$ determination at C7 similarly varied around COR_{total}. The measurements at C6 were associated with more, albeit undetermined, uncertainty than at the other sites because of the truncated incubation, but the general similarity of COR_{total} and $COR_{sulfate}$ was clear. Thus, as is consistent with solid-phase metal distributions and incubation results, no role for dissimilatory Mn reduction was indicated and only a small role for Fe reduction seems likely (Table 4, Fig. 7). Even if all C oxidation in the upper 2 cm (40, 38, and 20 mmol m^{-2} d^{-1} at C7, C18, and C26) were through Fe reduction, the depletion time for poorly crystalline Fe(III) pools would be ~20 h at all sites (i.e. not much shorter than the entire short-term incubations). Thus, the lack of importance for Fe reduction was not due to a rapid initial depletion of Fe(III) during the incubations. Possible coupling of the Fe and S cycles is discussed below.

Nitrogen cycling—The ability of *Thioploca* filaments to concentrate NO_3^- in their central vacuole, together with the high population density of this organism, led to a unique N cycle in the shelf sediments (Fossing et al. 1995) with possible implications for other element cycles. Results from both whole-core squeezing and from extraction of dried sediment demonstrated NO_3^- contents up to 100 times larger than those of the pore water (Table 2). Analysis of a sample of sheathed *Thioploca* bundles confirmed their high NO_3^- content (Table 3), and this value of 0.44

mmol g^{-1} dry wt combined with biomass maxima of sheathed *Thioploca* of 0.3–1.5 mg dry wt cm^{-3} found near the surface at C7–C26 (Schulz 1995) yields NO_3^- contents of 0.13–0.66 μmol cm^{-3}, equivalent to pore-water concentrations of 120–600 μM. In an independent determination of biovolumes of *Thioploca* filaments (excluding sheaths), Schulz et al. (1996) found sharp maxima at 0–0.5-cm depth, with the highest value at C7 (12 mm^3 cm^{-3}), and estimated that the vacuole made up 85% of this volume. In conjunction with an average NO_3^- concentration in the vacuoles of 200 mM (L. P. Nielsen pers. comm.), this corresponds to a sediment concentration of 2 μmol cm^{-3} (or 2 mM). Both of these approaches give NO_3^- concentrations that are consistent with the sediment data, including the maximum at C7.

Although the depth-integrated NO_3^- consumption rates as measured during the incubations were low relative to the total sediment metabolism, they were high compared to denitrification rates from other offshore sediments (Table 8; Canfield 1993). This difference was further accentuated by the fact that, as apparent from the time course at C18 (Fig. 14), the mean NO_3^- consumption rates during the incubations probably underestimated the initial rates. There was, however, a good agreement between the depth-integrated NO_3^- consumption rate (Table 8) and the sediment NO_3^- uptake determined in situ at C18 (2.1 mmol m^{-2} d^{-1}; Fossing et al. 1995). The benthic NO_3^- uptake might, however, vary strongly in time, since this uptake seems to be regulated by *Thioploca* in a complex manner (Fossing et al. 1995; Hüttel et al. 1996).

It has been proposed that *Thioploca* performs H_2S oxidation with NO_3^- in two steps (Fossing et al. 1995):

$$5H_2S + 2NO_3^- + 2H^+ \rightarrow 5S^0 + N_2 + 6H_2O \quad (5)$$

$$6NO_3^- + 5S^0 + 2H_2O \rightarrow 3N_2 + 5SO_4^{2-} + 4H^+ \quad (6)$$

$$\Sigma: 5H_2S + 8NO_3^- \rightarrow 5SO_4^{2-} + 4N_2 + 2H^+ + 4H_2O \quad (7)$$

The assumption that S^0 is an intermediate in H_2S oxidation by *Thioploca* arises from the observation of S^0 globules in the cells (Maier and Gallardo 1984*a*,*b*). We also found a high S content in *Thioploca* (Table 3), which we assume represents mainly S^0. In the sediment, this S content was equivalent to maximum concentrations of 0.5–2.7 μmol cm^{-3} that were determined by using the biomass estimates of Schulz (1995, *see above*). Thus, *Thioploca* accounted for up to 50% of the total sediment S^0 (surface values 5–10 μmol cm^{-3}; Fig. 8) but generally accounted for less than this.

The possible rates of H_2S oxidation to SO_4^{2-} (Eq. 7) that can be calculated from the depth-integrated NO_3^- consumption rates (Table 8) correspond to 4, 5, and 2% of the SO_4^{2-} reduction rates at C7, C18, and C26, respectively. Thus, only a small part of the H_2S produced during the incubations could have been reoxidized with NO_3^-, except possibly in the extremely NO_3^--rich 0–0.5-cm interval at C7.

The metabolic characteristics of *Thioploca* have not been determined directly, and it is possible that the observed NO_3^- consumption during our incubations was due to reactions other than complete oxidation of H_2S. Thus, the steps suggested for the oxidation (Eq. 5 and 6) need not be closely linked. Partial oxidation to S^0 could have been preferred during the incubations, in which case 4 times more H_2S would have been reacted than by complete oxidation (Eq. 7). If the $S:NO_3^-$ ratio of the *Thioploca* sample of 4 : 1 (Table 3) was representative of the *Thioploca* composition in general, the NO_3^- consumption could have been entirely coupled to oxidation of the internal S^0 pool (Eq. 6). Furthermore, it is possible that NO_3^- is reduced to NH_4^+ rather than to N_2, which would increase the oxidative capacity of the NO_3^- pool by 60% ($NO_3^- + 5\ e^- \rightarrow \frac{1}{2}N_2$; $NO_3^- + 8\ e^- \rightarrow NH_4^+$). This pathway could contribute to the low $\Sigma CO_2 : NH_4^+$ accumulation ratios near the surface at C7 and C18 (Table 6) and could also explain the high initial concentration of NH_4^+ relative to ΣCO_2 at those stations (Fig. 3). At C26 on the other hand, high $\Sigma CO_2 : NH_4^+$ accumulation ratios coincided with high NO_3^- consumption rates (Table 8). Hence, nonsystematic liberation ratios of ΣCO_2 to NH_4^+ in NO_3^--rich samples could result from differences in the organic matter being mineralized and make conclusions on the product of NO_3^- reduction difficult to support.

Fate of H_2S--We were surprised to find the combination of extreme rates of SO_4^{2-} reduction and low levels of H_2S in all shelf sediments except C6 (Fig. 3). With SO_4^{2-} reduction rates up to 1,500 nmol cm^{-3} d^{-1}, the maintenance of H_2S below detection (<1 μM) requires a half-life of <1 min. The subsurface maxima of a few micromoles observed in one core from C18 thus indicated a very delicate balance of production and consumption. As discussed above, the NO_3^- consumption rates (Table 8) were too small for oxidation with NO_3^- (Eq. 5 or 7) to explain the "missing" H_2S during the incubations.

The dominance by Fe^{2+} in the pore waters (Fig. 3) and the accumulation of FeS during the prolonged incubations at C7 and C18 demonstrated that Fe minerals were important H_2S scavengers as they are in other, less active sediments, such as C40 and C41. Throughout the short-term incubations, sediments remained H_2S-free, with H_2S accumulation and Fe^{2+} depletion shortly after the beginning of the prolonged incubations (i.e. after ~2 d). With H_2S removal according to Eq. 4, 25–38 mmol Fe(III) m^{-2} were required to scavenge the H_2S produced at the mean SO_4^{2-} reduction rates (Table 5) during the short-term incubations at C7, C18, and C26. This corresponds to 25–40% of the poorly crystalline Fe(III) fraction (Table 4). In addition to reaction with Fe(III), H_2S may also be removed by precipitation with Fe(II), particularly the quantitatively significant pool of nonsulfide Fe(II) found in the solid phase (compare Figs. 7, 8; Thamdrup et al. 1994*a*).

If Fe phases were as important scavengers of H_2S in situ as was the case during our incubations, this would imply that we sampled both C7 and C18 just 2 d before a buildup of H_2S (assuming that the Fe pool not was rapidly recycled in situ). In the absence of O_2 and Mn oxides, reoxidation of dissolved or particulate Fe(II) could

only be by NO_3^-. This process has been implied in hemipelagic sediments (Froelich et al. 1979) and has recently been demonstrated in pure cultures of marine bacteria (Straub et al. 1996). As argued above, however, the sediment NO_3^- uptake mainly went to *Thioploca,* and this organism is not considered an Fe oxidizer. Thus, rapid in situ cycling of the small Fe(III) fraction was unlikely at the time of the cruise. Eleven days passed between the first (C18; 12 March) and last (C26; 23 March) sampling, but we did not return to the same station during this interval. Ferdelman et al. (in prep.) measured 250 μM H_2S at 5-cm depth at a station 5.6 km seaward of C18 on 22 March and 400 μM H_2S at the sediment–water interface of C7 on 27 March, 6 d after our sampling. Also, strong sulfide smell has previously been reported from the surface sediments (Gallardo 1977) where we detected no H_2S, so H_2S fluctuations may be common, and it is possible that a H_2S buildup was imminent.

We cannot exclude the possibility that the *Thioploca* in the shelf sediments contributed more significantly to H_2S scavenging in situ than was the case during the incubations. The NO_3^- uptake of the sediments could be experimentally increased well beyond the consumption rates measured during our incubations (Table 8; Fossing et al. 1995; Hüttel et al. 1996), but it is yet unknown how this uptake is regulated under natural conditions. However, the distribution of SO_4^{2-} reduction rates (Fig. 13) relative to the pore-water chemistry (Fig. 3) indicates that for *Thioploca* to quantitatively dominate H_2S scavenging, it has to compete efficiently for H_2S at < 1 μM levels with rapid reactions that involve Fe(III) and Fe(II). This would require a close association between *Thioploca* and the H_2S-producing SO_4^{2-} reducers.

Conclusion

Sulfate reduction was the dominant pathway of C oxidation at all sites along the transect of the Chilean margin. In the shelf sediments, sulfate reduction accounted for essentially all mineralization, whereas the importance of other e^- acceptors increased down the slope, where Fe reduction became the second most important pathway, contributing 29% of C oxidation at 2,000 m depth (Table 10). Conditions on the shelf were extreme with respect to both total mineralization rates and the lack of O_2 in the bottom water, whereas the slope sites fell within the typical range of coastal sediments in these respects.

Our observations, add to the small database that supports the general importance of Fe (and in some cases Mn) reduction in sedimentary C oxidation. Significant Fe reduction was dependent on the presence of poorly crystalline Fe(III), which is in agreement with observations in enrichment cultures (Lovley and Phillips 1986). In sediment slurries, Fe-reducing bacteria were found to efficiently outcompete SO_4^{2-} reducers for common substrates (Lovley and Phillips 1987). In the slope sediments, however, zones of Fe and SO_4^{2-} reduction overlapped, as has also been observed in sediments of the Norwegian Trough (Canfield et al. 1993*b*). Furthermore, rates of SO_4^{2-} reduction increased concomitantly with the depletion of poorly crystalline Fe(III) with depth, suggesting that rates of Fe reduction are limited by Fe(III) availability in such sediments. The co-occurrence of Fe and SO_4^{2-} reduction complicates the Fe cycle because Fe reducers must compete for Fe(III) with reactions that involve H_2S. The outcome of this competition likely depends on the reactivity of both the available Fe(III) and C_{org}.

Because of the particulate nature of both Fe and Mn oxides and solid Fe(II) and Mn(II) phases, physical mixing of sediments is necessary to recycle the metals and support significant reduction rates, and mixing additionally stimulates anaerobic mineralization by burial of reactive C_{org} below the oxic zone (Aller 1990; Canfield et al. 1993*b*). Apart from shallow sediments where reworking by waves and currents can be important (Aller et al. 1996), bioturbation is therefore a key process in the regulation of metal reduction rates. A recent compilation of intensities and depths of mixing in sediments from the coast to the deep sea gives a worldwide mean mixing depth of 9.8 ± 4.5 cm (Boudreau 1994). Because O_2 and NO_3^- typically penetrate only a few millimeters to centimeters into shelf and slope sediments (e.g. Jørgensen and Revsbech 1989; Reimers et al. 1992; Glud et al. 1994; Brandes and Devol 1995), significant Fe reduction could be widespread on the continental margins. However, mixing intensities, which have been estimated by assuming diffusional transport, vary by several orders of magnitude between sites, and the actual modes of mixing are poorly understood (Boudreau 1994). Further quantitative studies of bioturbation are therefore important for a better understanding of the regulation and general importance of Fe reduction in sediments.

References

AHUMADA, R., A. RUDOLPH, AND V. MARTINEZ. 1983. Circulation and fertility of waters in Concepcion Bay. Estuarine Coastal Shelf Sci. **16:** 95–105.

ALLER, R. C. 1980. Diagenetic processes near the sediment-water interface of Long Island Sound. 2. Fe and Mn. Adv. Geophys. **22:** 351–415.

———. 1990. Bioturbation and manganese cycling in hemipelagic sediments. Phil. Trans. R. Soc. Lond. Ser. A **331:** 51–58.

———. 1994. The sedimentary Mn cycle in Long Island Sound: Its role as intermediate oxidant and the influence of bioturbation, O_2, and C_{org} flux on diagenetic reaction balances. J. Mar. Res. **52:** 259–295.

———, N. E. BLAIR, Q. XIA, AND P. D. RUDE. 1996. Remineralization rates, recycling, and storage of carbon in Amazon shelf sediments. Cont. Shelf Res. **16:** 753–786.

ALPERIN, M. J., D. B. ALBERT, AND C. S. MARTENS. 1994. Seasonal variation in production and consumption rates of dissolved organic carbon in an organic-rich coastal sediment. Geochim. Cosmochim. Acta **58:** 4909–4930.

ANDERSON, L. A., AND J. L. SARMIENTO. 1994. Redfield ratios of remineralization determined by nutrient data analysis. Global Biogeochem. Cycles **8:** 65–80.

ARCOS, D. F., AND R. E. WILSON. 1984. Upwelling and the distribution of chlorophyll *a* within the Bay of Concepción, Chile. Estuarine Coastal Shelf Sci. **18:** 25–35.

BARNETT, P. R. O., J. WATSON, AND D. CONELLY. 1984. A multiple corer for taking virtually undisturbed samples from shelf, bathyal, and abyssal sediments. Ocean. Acta **7:** 399–408.

BENDER, M. L., AND D. T. HEGGIE. 1984. Fate of organic carbon reaching the deep sea floor: A status report. Geochim. Cosmochim. Acta **48:** 977–986.

———, AND OTHERS. 1987. A whole-core squeezer for interstitial pore-water sampling. Limnol. Oceanogr. **32:** 1214–1225.

BERNER, R. A. 1980. Early diagenesis, a theoretical approach. Princeton.

BRANDES, J. A., AND A. H. DEVOL. 1995. Simultaneous nitrate and oxygen respiration in coastal sediments: Evidence for discrete diagenesis. J. Mar. Res. **53:** 771–797.

BRANDHORST, W. 1959. Relationship between the hake fisheries and a southerly subsurface return flow below the Perú Coastal Current off the Chilean coast. Nature **183:** 1832–1833.

BOUDREAU, B. P. 1994. Is burial velocity a master parameter for bioturbation? Geochim. Cosmochim. Acta **58:** 1243–1249.

———, D. E. CANFIELD, AND A. MUCCI. 1992. Early diagenesis in a marine sapropel, Mangrove Lake, Bermuda. Limnol. Oceanogr. **37:** 1738–1753.

BURDIGE, D. J., AND K. H. NEALSON. 1986. Chemical and microbiological studies of sulfide-mediated manganese reduction. Geomicrobiol. J. **4:** 361–387.

CANFIELD, D. E. 1988. Sulfate reduction and the diagenesis of iron in anoxic marine sediments. Ph.D. thesis, Yale Univ. 248 p.

———. 1989. Reactive iron in sediments. Geochim. Cosmochim. Acta **53:** 619–632.

———. 1993. Organic matter oxidation in marine sediments, p. 333–363. *In* R. Wollast et al. [eds.]. Interactions of C, N, P and S biogeochemical cycles. Springer.

———, AND D. J. DES MARAIS. 1991. Aerobic sulfate reduction in microbial mats. Science **251:** 1471–1473.

———, B. B. JØRGENSEN, AND OTHERS. 1993*a*. Pathways of organic carbon oxidation in three coastal sediments. Mar. Geol. **113:** 27–40.

———, R. RAISWELL, AND S. BOTTRELL. 1992. The reactivity of sedimentary iron minerals towards sulfide. Am. J. Sci. **292:** 659–683.

———, ———, J. T. WESTRICH, C. M. REAVES, AND R. A. BERNER. 1986. The use of chromium reduction in the analysis of reduced inorganic sulfur in sediments and shales. Chem. Geol. **54:** 149–155.

———, B. THAMDRUP, AND J. W. HANSEN. 1993*b*. The anaerobic degradation of organic matter in Danish coastal sediments. Geochim. Cosmochim. Acta **57:** 3867–3883.

CLINE, J. D. 1969. Spectrophotometric determination of hydrogen sulfide in natural waters. Limnol. Oceanogr. **14:** 454–458.

CRILL, P. M., AND C. S. MARTENS. 1987. Biogeochemical cycling in an organic-rich coastal marine basin. 6. Temporal and spatial variations in sulfate reduction rates. Geochim. Cosmochim. Acta **51:** 1175–1186.

DEVOL, A. H., AND J. P. CHRISTENSEN. 1993. Benthic fluxes and nitrogen cycling in the sediments of the continental margin of the eastern North Pacific. J. Mar. Res. **51:** 345–372.

FISCHER, W. R. 1973. Die Wirkung von zweiwertigem Eisen auf Lösung und Umwandlung von Eisen (III)-hydroxiden, p. 37–44. *In* E. Schlichting and U. Schwertmann [eds.], Pseudogley and gley: Genesis and use of hydromorphic soils. Weinheim.

FOSSING, H. 1990. Sulfate reduction in shelf sediments in the upwelling region off central Peru. Cont. Shelf Res. **10:** 355–367.

———, V. A. GALLARDO, AND OTHERS. 1995. Concentration and transport of nitrate by the mat-forming sulphur bacterium *Thioploca*. Nature **374:** 713–715.

———, AND B. B. JØRGENSEN. 1989. Measurement of bacterial sulfate reduction in sediments: evaluation of a single-step chromium reduction method. Biogeochemistry **8:** 223–245.

FROELICH, P. N., M. A. ARTHUR, AND OTHERS. 1988. Early diagenesis of organic matter in Peru continental margin sediments: Phosphorite precipitation. Mar. Geol. **80:** 309–343.

———, G. P. KLINKHAMMER, AND OTHERS. 1979. Early oxidation of organic matter in pelagic sediments of the eastern equatorial Atlantic: Suboxic diagenesis. Geochim. Cosmochim. Acta **43:** 1075–1090.

GALLARDO, V. A. 1977. Large benthic microbial communities in sulfide biota under the Peru-Chile subsurface countercurrent. Nature **268:** 331–332.

GLUD, R. N., J. K. GUNDERSEN, B. B. JØRGENSEN, N. P. REVSBECH, AND H. D. SCHULZ. 1994. Diffusive and total oxygen uptake of deep-sea sediments in the south east Atlantic Ocean: In situ and laboratory measurements. Deep-Sea Res. **41:** 1767–1788.

GOLDHABER, M. B., AND I. R. KAPLAN. 1974. The sulfur cycle, p. 569–655, *In* E. D. Goldberg [ed.], The sea. V. 5. Wiley.

GUNDERSEN, J. K., AND B. B. JØRGENSEN. 1991. Fine-scale in situ measurements of oxygen distribution in marine sediments. Kiel. Meeresforsch. Sonderh. **8:** 376–380.

HALL, P. O. J., AND R. C. ALLER. 1992. Rapid, small-volume, flow injection analysis for ΣCO_2 and NH_4^+ in marine and freshwaters. Limnol. Oceanogr. **37:** 1113–1119.

HANSEN, J. W. 1992. The ecological significance of manganese in marine sediments [in Danish]. M.S. thesis, Univ. Aarhus. 87 p.

HENRICHS, S. M. 1992. Early diagenesis of organic matter in marine sediments: Progress and perplexity. Mar. Chem. **39:** 119–149.

———, AND W. S. REEBURGH. 1987. Anaerobic mineralization of marine organic matter: Rates and the role of anaerobic processes in the ocean carbon economy. Geomicrobiol. J. **5:** 191–237.

HINES, M. E., D. A. BAZYLINSKI, J. B. TUGEL, AND W. B. LYONS. 1991. Anaerobic microbial biogeochemistry in sediments from two basins in the Gulf of Maine: Evidence for iron and manganese reduction. Estuarine Coastal Shelf Sci. **32:** 313–324.

HÜTTEL, M., S. FORSTER, S. KLÖSER, AND H. FOSSING. 1996. Overcoming diffusive limitations: Vertical migration in the sediment-living sulfur bacterium *Thioploca* spp. Appl. Environ. Microbiol. **62:** 1863–1872.

JONES, M. N. 1984. Nitrate reduction by shaking with cadmium. Water Res. **18:** 643–646.

JØRGENSEN, B. B. 1978. A comparison of methods for the quantification of bacterial sulfate reduction in coastal marine sediments. 1. Measurement with radiotracer techniques. Geomicrobiol. J. **1:** 11–28.

———. 1982. Mineralization of organic matter in the sea bed—the role of sulfate reduction. Nature **296:** 643–645.

———, AND Y. COHEN. 1977. Solar Lake (Sinai). 5. The sulfur

cycle of the benthic cyanobacterial mats. Limnol. Oceanogr. **22:** 657–666.

———, AND N. P. REVSBECH. 1989. Oxygen uptake, bacterial distribution, and carbon-nitrogen-sulfur cycling in sediments from the Baltic Sea–North sea transition. Ophelia **31:** 29–49.

KEIR, R. S. 1980. The dissolution kinetics of biogenic calcium carbonate in seawater. Geochim. Cosmochim. Acta **44:** 241–252.

KOSTKA, J. E., AND G. W. LUTHER III. 1994. Partitioning and speciation of solid phase iron in saltmarsh sediments. Geochim. Cosmochim. Acta **58:** 1701–1710.

KRISTENSEN, E., S. I. AHMED, AND A. H. DEVOL. 1995. Aerobic and anaerobic decomposition of organic matter in marine sediment: Which is fastest? Limnol. Oceanogr. **40:** 1430–1437.

KRUSE, B. 1993. Measurement of plankton O_2 respiration in gas-tight plastic bags. Mar. Ecol. Prog. Ser. **94:** 155–163.

LORD, C. J., III. 1980. The chemistry and cycling of iron, manganese, and sulfur in salt marsh sediments. Ph.D. thesis, Univ. Delaware.

LOVLEY, D. R., AND E. J. P. PHILLIPS. 1986. Availability of ferric iron for microbial reduction in bottom sediments of the freshwater tidal Potomac River. Appl. Environ. Microbiol. **52:** 751–757.

———, AND ———. 1987. Competitive mechanisms for inhibition of sulfate reduction and methane production in the zone of ferric iron reduction in sediments. Appl. Environ. Microbiol. **53:** 2636–2641.

MACKIN, J. E., AND R. C. ALLER. 1984. Ammonium adsorption in marine sediments. Limnol. Oceanogr. **29:** 250–257.

MAIER, S., AND V. A. GALLARDO. 1984*a*. Description of *Thioploca araucae* sp. nov. and *Thioploca chilea* sp. nov. Int. J. Syst. Bacteriol. **34:** 414–418.

———, AND ———. 1984*b*. Nutritional characteristics of two marine Thioplocas determined by autoradiography. Arch. Microbiol. **139:** 218–220.

MARTENS, C. S., AND J. V. KLUMP. 1984. Biogeochemical cycling in an organic rich coastal marine basin. 4. An organic carbon budget for sediments dominated by sulfate reduction and methanogenesis. Geochim. Cosmochim. Acta **48:** 1987–2004.

MEHRBACH, C., C. H. CULBERSON, J. E. HARVEY, AND R. M. PYTKOWICZ. 1973. Measurement of the apparent dissociation constants of carbonic acid in seawater at atmospheric pressure. Limnol. Oceanogr. **18:** 897–907.

MORSE, J. 1978. Dissolution kinetics of calcium carbonate in seawater. 4: The near-equilibrium dissolution kinetics of calcium carbonate-rich deep-sea sediments. Am. J. Sci. **278:** 344–355.

MUCCI, A. 1983. The solubility of calcite and aragonite in seawater at various salinities, temperatures, and one atmosphere total pressure. Am. J. Sci. **283:** 780–799.

NIELSEN, L. P. 1992. Denitrification in sediment determined from nitrogen isotope pairing. FEMS Microb. Ecol. **86:** 357–362.

PARKES, R. J., G. R. GIBSON, I. MUELLER-HARVEY, W. J. BUCKINGHAM, AND R. A. HERBERT. 1989. Determination of the substrates for sulphate-reducing bacteria within marine and estuarine sediments with different rates of sulphate reduction. J. Gen. Microbiol. **135:** 175–187.

PETERSON, W. T., AND OTHERS. 1988. The nearshore zone during coastal upwelling: Daily variability between primary and secondary production off central Chile. Prog. Oceanogr. **20:** 1–40.

PHILLIPS, E. J. P., AND D. R. LOVLEY. 1987. Determination of Fe(III) and Fe(II) in oxalate extracts of sediments. Soil Sci. Soc. Am. J. **51:** 938–941.

POSTMA, D. 1985. Concentration of Mn and separation from Fe in sediments–1. Kinetics and stoichiometry of the reaction between birnessite and dissolved Fe(II) at 10°C. Geochim. Cosmochim. Acta **49:** 1023–1033.

PYZIK, A. J., AND S. E. SOMMER. 1981. Sedimentary iron monosulfides: Kinetics and mechanism of formation. Geochim. Cosmochim. Acta **45:** 687–698.

RAISWELL, R., D. E. CANFIELD, AND R. A. BERNER. 1994. A comparison of iron extraction methods for the determination of degree of pyritization and the recognition of iron-limited pyrite formation. Chem. Geol. **111:** 101–110.

REDFIELD, A. C., B. H. KETCHUM, AND F. A. RICHARDS. 1963. The influence of organisms on the composition of sea-water, p. 26–77. *In* M. N. Hill [ed.], The sea. V. 2. Wiley Interscience.

REIMERS, C. E., R. A. JAHNKE, AND D. C. MCCORKLE. 1992. Carbon fluxes and burial rates over the continental slope and rise off central California with implications for the global carbon cycle. Global Biogeochem. Cycles **6:** 199–224.

ROA, R., AND OTHERS. 1995. Nursery ground, age structure and abundance of juvenile squat lobster *Pleuroncodes monodon* on the continental shelf off central Chile. Mar. Ecol. Prog. Ser. **116:** 47–54.

ROSENFELD, J. K. 1979. Ammonium adsorption in nearshore anoxic sediments. Limnol. Oceanogr. **24:** 356–364.

SCHINK, B. 1988. Principles and limits of anaerobic degradation: Environmental and technological aspects p. 771–846. *In* A. J. B. Zehnder [ed.], Biology of anaerobic microorganisms. Wiley.

SCHULZ, H. 1995. Zur Struktur der *Thioploca*-Gemeinschaft auf dem Schelf vor Concepción/Chile. M.S. thesis, Univ. Bremen. 69 p.

———, B. B. JØRGENSEN, H. FOSSING, AND N. B. RAMSING. 1996. Community structure of filamentous, sheath-building sulfur bacteria, *Thioploca* spp., off the coast of Chile. Appl. Environ. Microbiol. **62:** 1855–1862.

SCHWERTMANN, U. 1964. Differenzierung der Eisenoxide des Bodens durch Extraktion mit Ammoniumoxalat-Lösung. Z. Pflanzen. Bodenk. **105:** 194–202.

SEITZINGER, S. P., S. W. NIXON, AND M. E. Q. PILSON. 1984. Denitrification and nitrous oxide production in a coastal marine ecosystem. Limnol. Oceanogr. **29:** 73–83.

SOBARZO, M. A. 1994. Oceanografia fisica entre Punta Nugurne (35°57′S; 72°47′W) y Punta Manuel (38°30′S; 73°31′W), Chile: Una revision historica (1936–1990). Gayana Oceanol. **2:** 5–17.

SØRENSEN, J. 1978. Denitrification rates in a marine sediment as measured by the acetylene inhibition technique. Appl. Environ. Microbiol. **43:** 319–324.

———. 1982. Reduction of ferric iron in anaerobic, marine sediment and interaction with reduction of nitrate and sulfate. Appl. Environ. Microbiol. **43:** 319–324.

———, D. CHRISTENSEN, AND B. B. JØRGENSEN. 1981. Volatile fatty acids and hydrogen as substrates for sulfate-reducing bacteria in anaerobic marine sediments. Appl. Environ. Microbiol. **42:** 5–11.

———, AND B. B. JØRGENSEN. 1987. Early diagenesis in sediments from Danish coastal waters: Microbial activity and Mn-Fe-S geochemistry. Geochim. Cosmochim. Acta **51:** 1583–1590.

———, ———, AND N. P. REVSBECH. 1979. A comparison of oxygen, nitrate, and sulfate respiration in coastal marine sediments. Microb. Ecol. **5:** 105–116.

STOOKEY, L. L. 1970. Ferrozine—a new spectrophotometric reagent for iron. Anal. Chem. **42:** 779–781.

STRAUB, K. L., M. BENZ, B. SCHINK, AND F. WIDDEL. 1996. Anaerobic, nitrate-dependent microbial oxidation of ferrous iron. Appl. Environ. Microbiol. **62:** 1458–1460.

SUTER, D., C. SIFFERT, B. SULZBERGER, AND W. STUMM. 1988. Catalytic dissolution of iron(III) (hydr)oxides by oxalic acid in the presence of Fe(II). Naturwissenschaften **75:** 571–573.

TESKE, A., N. B. RAMSING, J. KÜVER, AND H. FOSSING. 1996. Phylogeny of *Thioploca* and related filamentous sulfide-oxidizing bacteria. Syst. Appl. Microbiol. **18:** 517–526.

THAMDRUP, B., H. FOSSING, AND B. B. JØRGENSEN. 1994a. Manganese, iron, and sulfur cycling in a coastal marine sediment, Aarhus Bay, Denmark. Geochim. Cosmochim. Acta **58:** 5115–5129.

———, R. N. GLUD, AND J. W. HANSEN. 1994b. Manganese oxidation and in situ manganese fluxes from a coastal sediment. Geochim. Cosmochim. Acta **58:** 2563–2570.

WESTRICH, J. T. 1983. The consequences and controls of bacterial sulfate reduction in marine sediments. Ph.D. thesis, Yale Univ.

———, AND R. A. BERNER. 1984. The role of sedimentary organic matter in bacterial sulfate reduction: The *G* model tested. Limnol. Oceanogr. **29:** 236–249.

ZHABINA, N. N., AND I. I. VOLKOV. 1978. A method of determination of various sulfur compounds in sea sediments and rocks, p. 735–746. *In* W. E. Krumbein [ed.], Environmental biogeochemistry and geomicrobiology. V. 3. Ann Arbor Sci.

Submitted: 22 January 1996
Accepted: 2 April 1996
Amended: 12 June 1996